A whole-brain map of long-range inputs to GABAergic interneurons in the mouse medial prefrontal cortex

Qingtao Sun[1,2,6], Xiangning Li[1,2,3,6], Miao Ren[1,2], Mengting Zhao[1,2], Qiuyuan Zhong[1,2], Yuqi Ren[4], Pan Luo[1,2], Hong Ni[1,2], Xiaoyu Zhang[1,2], Chen Zhang[1,2], Jing Yuan[1,2,3], Anan Li[1,2,3,5], Minmin Luo[4], Hui Gong[1,2,3,5] and Qingming Luo[1,2,3]*

The medial prefrontal cortex (mPFC) contains populations of GABAergic interneurons that play different roles in cognition and emotion. Their local and long-range inputs are incompletely understood. We used monosynaptic rabies viral tracers in combination with fluorescence micro-optical sectioning tomography to generate a whole-brain atlas of direct long-range inputs to GABAergic interneurons in the mPFC of male mice. We discovered that three subtypes of GABAergic interneurons in two areas of the mPFC are innervated by same upstream areas. Input from subcortical upstream areas includes cholinergic neurons from the basal forebrain and serotonergic neurons (which co-release glutamate) from the raphe nuclei. Reconstruction of single-neuron morphology revealed novel substantia innominata–anteromedial thalamic nucleus–mPFC and striatum–anteromedial thalamic nucleus–mPFC circuits. Based on the projection logic of individual neurons, we classified cortical and hippocampal input neurons into several types. This atlas provides the anatomical foundation for understanding the functional organization of the mPFC.

GABAergic neurons in the mPFC play an important role in regulating working memory, decision-making and emotion associated with motivational and aversive behaviors[1,2], and their dysfunction has been implicated in various diseases, including major depression, schizophrenia and epilepsy[3–5]. Subtypes of GABAergic neurons in the mPFC include parvalbumin-expressing (PV+), somatostatin-expressing (SST+) and vasoactive intestinal peptide-expressing (VIP+) neurons, which have different functions at the circuit and behavior levels[2,6]. To better understand their specific functions, it is helpful to know the inputs to these interneuron subtypes, especially the direct synaptic inputs at the whole-brain level.

Conventional tracing studies using chemical neural tracers or adeno-associated virus indicated that mPFC receives massive inputs from cortical and subcortical nuclei[7–9], but these tracing methods are unable to demonstrate neural inputs to specific types of neurons. Studies using paired recordings have indicated that PV+, SST+ and VIP+ interneurons receive inputs from various cell types in local circuits[6], but such recordings can only resolve the connections within local circuits or columns. Studies using optogenetic-assisted circuit mapping found that PV+ neurons in the mPFC receive direct PV+ inputs from the basal forebrain and dopaminergic inputs from the ventral tegmental area (VTA)[10,11], as well as direct inputs from the limbic thalamus to drive feed-forward inhibition[12]. Although optogenetic technology can demonstrate the long-range connectivity of specific neuron types, it cannot easily identify neural connections among multiple brain areas. The genetic modified rabies virus (RV) tracing makes it possible to analyze the long-range inputs of specific neurons[13,14], but detailed characterization of the

long-range input neurons and, in particular, of the collateral projections of these input neurons requires precise imaging along with cytoarchitectonic information in the whole brain.

With a fluorescence micro-optical sectioning tomography system (fMOST)[15], we employed modified rabies virus tracing in Cre driver mice to investigate the long-range inputs to PV+, SST+ and VIP+ neurons in the prelimbic (PL) and infralimbic (ILA) areas, which are two subregions of the mPFC with different functions[16]. We identified the distribution patterns of direct input neurons that target different GABAergic neurons. By analyzing the neurochemical properties and the morphology of individual neurons, we uncovered several circuits and types of neurons that control GABAergic neurons in the mPFC. To better present the raw data, we also developed interactive online representations of the whole-brain distribution, proportions of the input neurons and the reconstructions of the input neurons in the neocortex and hippocampus for readers to access and download (http://eai.brainsmatics.org/brainsweb-simple/index.html). Overall, we have provided a comprehensive whole-brain atlas of direct long-range inputs to different GABAergic neurons in the mPFC, which will lead to deep insights into the structural and functional organization of prefrontal cortex.

Results

Whole-brain visualization of long-range input neurons with RV and fMOST. To label the monosynaptic input neurons of GABAergic neurons in the mPFC, we first injected two Cre-dependent helper viruses, AAV-DIO-TVA-mCherry and AAV-DIO-RG, into the prelimbic or infralimbic area of the mPFC (Fig. 1a). These helper viruses provide the receptor that allows
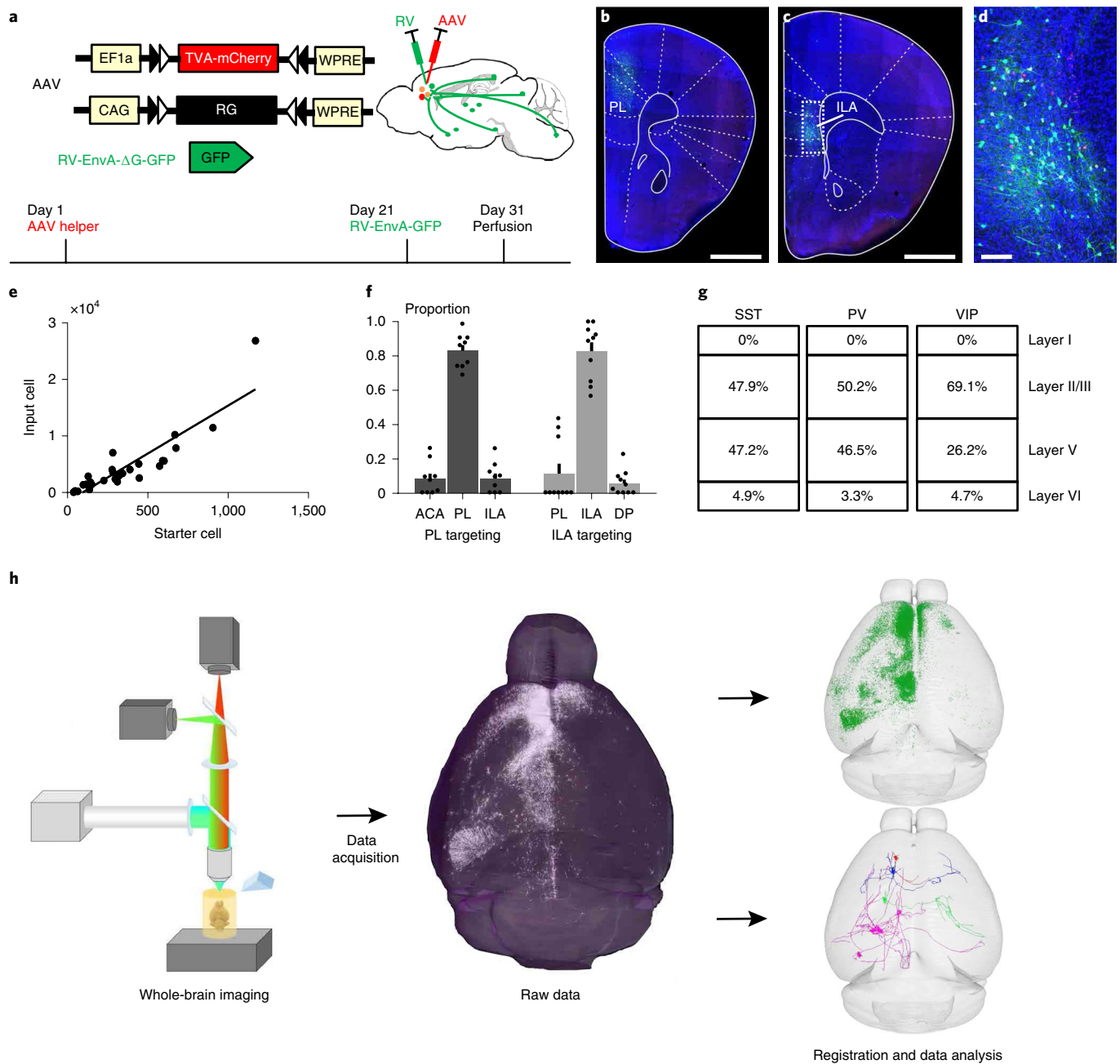
Fig. 1 | Characterization of monosynaptic inputs to three types of interneurons in different subregions of the mPFC. a, AAV helper virus and genetically modified rabies virus pseudotyped with EnvA. The *RG* gene is replaced by *EGFP*. The experimental strategy and time line are shown on the right and below. **b,c**, Characterization of the injection site at the PL (**b**) and ILA areas (**c**). **d**, Enlarged image of boxed area in **c** showing the starter cells (yellow) and local input cells (green). **e**, Relationship between starter cell and long-range input cells; 28 mice were used for the analysis. Units indicate numbers of neurons. **f**, Distribution of the starter cells in each cortical area when targeting the PL or ILA areas; 9 mice with PL targeting and 10 mice with ILA targeting were used for the analysis. **g**, Layer distribution of starter cells. SST+, $n = 12$ mice; PV+, $n = 8$ mice; VIP+, $n = 8$ mice. **h**, Main steps of data generation and processing. The virus-labeled samples were imaged using a whole-brain imaging system, and the raw data were analyzed and registered to the Allen CCF v.3.0. Scale bars, **b,c**, 1 mm; **d**, 100 μm. ACA, anterior cingulate area; DP, dorsal peduncular area.

EnvA-coated RV to enter the Cre-positive neurons and glycoprotein for RV to transfer to the monosynaptic input neurons. After 3–4 weeks, SAD-ΔG-GFP (EnvA)-RV was injected into the same site (Fig. 1a). After 10 d, we identified massive green fluorescent protein (GFP)-labeled neurons and dual-color-labeled neurons at the injection site (Fig. 1b–d). The dual-color-labeled neurons were defined as starter cells as in previous studies[17,18]. Substantial numbers of neurons in different brain areas were also labeled by RV. Although the numbers of labeled neurons were variable, there was

a correlation between the number of input neurons and starter cells (Fig. 1e and Supplementary Table 1).

To examine the specificity of the virus tracing, we performed immunochemical staining against PV or SST at the injection site. We found most of the mCherry-labeled neurons were PV+ (679 of 760, $n = 6$) or SST+ (238 of 272, $n = 6$) (Supplementary Fig. 1a,b). To evaluate potential leakage expression of the virus, we performed control experiments. When we only injected SAD-ΔG-GFP (EnvA)-RV into the mouse brain, no neuron was

labeled (Supplementary Fig. 1c–e). When we injected AAV-DIO-TVA-mCherry and SAD-ΔG-GFP (EnvA)-RV into the mPFC of PV-Cre mice, only neurons at the injection site were labeled (Supplementary Fig. 1f). More than 92% of the labeled neurons were PV+ (Supplementary Fig. 1g–k). When we injected AAV-DIO-TVA-mCherry, AAV-DIO-RG and SAD-ΔG-GFP(EnvA)-RV in wild-type mice, only a few neurons were labeled at the injection site (101 ± 22, $n = 3$, mean $\pm$ s.e.m.) and no neuron was labeled outside the injection site (Supplementary Fig. 1l–n). Here, when we calculated the number of input neurons, we excluded neurons around the injection site. To examine whether the virus was delivered into the correct subregions of the mPFC, we counted the distribution of the starter cells in the PL and ILA areas. Most of the starter cells remained within the injection site and only a few cells spread into the adjacent cortical areas (Fig. 1f and Supplementary Table 1).

We also analyzed the layer distribution of the starter cells to examine whether there was layer-distribution bias of the starter cells. Most starter cells in the PV-Cre and SST-Cre mice were located in layers II, III and V, while the starter cells in the VIP-Cre mice were mainly located in layers II and III and a few in layer V and VI (Fig. 1g and Supplementary Table 1). The layer distributions of these starter cells were similar to that of PV+, SST+ and VIP+ neurons in the mPFC (Supplementary Fig. 2 and Supplementary Table 2).

To acquire the whole-brain distribution and the projectome of the input neurons, we performed precise whole-brain imaging (Fig. 1h). Briefly, the virus-labeled brain samples were embedded in resin and imaged at a resolution of $0.32 \times 0.32 \times 2 \, \mu m^3$ (Supplementary Fig. 3a,b). The raw data acquired from imaging were registered to the Allen Common Coordinate Framework (CCF) (Fig. 1h). A data set contained over 5,000 coronal slices. These submicrometer-resolution images indicate the finely detailed, single-neuron morphology of these input neurons.

Whole-brain distribution of monosynaptic inputs to PV+/SST+/VIP+ neurons in the PL and ILA areas. Using the precise imaging, we acquired the whole-brain data set of the neurons that send monosynaptic inputs to GABAergic neurons in the mPFC. Different GABAergic neurons in the PL and ILA areas received inputs from similar brain areas (Supplementary Fig. 3a). To determine whether the same neuron can simultaneously innervate the PL and ILA areas, we performed dual-color RV labeling. Three weeks after the injection of the helper virus AAV-DIO-hBFP-TVA/AAV-DIO-RG, we injected SAD-ΔG-GFP(EnvA)-RV and SAD-ΔG-DsRed(EnvA)-RV into PL and ILA, respectively. We identified GFP and DsRed-labeled neurons in individual brain areas. Only a few neurons were dual-color-labeled (Fig. 2a and Supplementary Fig. 4), indicating that the PL and ILA areas receive inputs from different neurons within the same brain areas. However, the number of dual-color RV-labeled neurons may be underestimated due to the super-infection exclusion and low efficiency of the RV tracing[19]. To further examine whether the PL and ILA areas are innervated by different neurons, we simultaneously injected conjugated retrograde tracer cholera toxin subunit b (CTb) into the PL and ILA areas (Supplementary Fig. 5a,b). Quantifying the number of CTb-labeled neurons in some major brain areas, we found that less than 10% of the CTb-labeled neurons innervated the PL and ILA areas simultaneously (Supplementary Fig. 5c–j and Supplementary Table 3). This result further demonstrated that the PL and ILA areas are innervated by different neurons in the same brain areas.

To understand the distribution patterns of the neurons that directly project to different types of GABAergic neurons in the mPFC, we calculated the proportions of these input neurons in each brain area (Fig. 2b and Supplementary Table 4). At the grouped anatomical level, the upstream areas included the neocortex, olfactory areas, claustrum, striatum, pallidum, amygdala, thalamus,

hypothalamus, hippocampal formation, midbrain and hindbrain (Supplementary Fig. 6). These results are consistent with conventional tracing studies[7–9]. The PV+ neurons in the mPFC (PV+$_{mPFC}$) received more cortical inputs than the SST+ neurons in the mPFC (SST+$_{mPFC}$) (Supplementary Fig. 6, PV+$_{PL}$ versus SST+$_{PL}$, $P = 0.019$; PV+$_{ILA}$ versus SST+$_{ILA}$, $P = 0.02$), while SST+$_{mPFC}$ received more inputs from subcortical nuclei than did PV+$_{mPFC}$ (Supplementary Fig. 6). The SST+ neurons in ILA (SST+$_{ILA}$) received more inputs from the striatum and pallidum than did PV+ neurons in ILA (PV+$_{ILA}$) (Supplementary Fig. 6, for striatum, PV+$_{ILA}$ versus SST+$_{ILA}$, $P < 0.0001$; for pallidum, PV+$_{ILA}$ versus SST+$_{ILA}$, $P = 0.027$).

We found that many brain areas had biases towards different GABAergic neurons in the mPFC. For example, the PV+$_{PL}$ (PV+ neurons in the PL area) received more inputs from the frontal association cortex ($P = 0.001$) and retrosplenial granular cortex ($P = 0.028$) than did SST+$_{PL}$ (SST+ neurons in the PL area) (Fig. 2b and Supplementary Fig. 7a,f). PV+$_{ILA}$ received more inputs from the cingulate cortex than did VIP+$_{ILA}$ (VIP+ neurons in the ILA area) (Fig. 2b, $P = 0.038$). The lateral orbital cortex preferentially innervated VIP+ neurons in both the PL and ILA areas (Fig. 2b, VIP+$_{PL}$ versus SST+$_{PL}$, $P < 0.0001$; VIP+$_{PL}$ versus PV+$_{PL}$, $P = 0.002$; VIP+$_{ILA}$ versus SST+$_{ILA}$, $P = 0.015$). The VIP+$_{mPFC}$ (VIP+ neurons in the mPFC) received more inputs from the secondary motor cortex than did SST+$_{mPFC}$ (Fig. 2b and Supplementary Fig. 7c, VIP+$_{PL}$ versus SST+$_{PL}$, $P = 0.043$; VIP+$_{ILA}$ versus SST+$_{ILA}$, $P = 0.047$). In the olfactory area, the SST+$_{PL}$ received more inputs from the anterior olfactory nucleus compared with PV+$_{PL}$ (Fig. 2b and Supplementary Fig. 7b). The VIP+$_{PL}$ (VIP+ neurons in the PL area) received more inputs from the dorsal peduncular cortex than did SST+$_{PL}$ (Fig. 2b). In striatum, the lateral septum preferentially innervated SST+$_{ILA}$ (Fig. 2b, PV+$_{ILA}$ versus SST+$_{ILA}$, $P = 0.001$; VIP+$_{ILA}$ versus SST+$_{ILA}$, $P = 0.009$). In pallidum, inputs from the nucleus of the diagonal band to SST+ neurons were larger than those to PV+ and VIP+ neurons (Fig. 2b and Supplementary Fig. 7d; for the vertical limb of the diagonal bands (VDB), PV+$_{PL}$ versus SST+$_{PL}$, $P = 0.008$, VIP+$_{PL}$ versus SST+$_{PL}$, $P = 0.004$, PV+$_{ILA}$ versus SST+$_{ILA}$, $P = 0.045$; for the horizontal limb of the diagonal band (HDB), PV+$_{PL}$ versus SST+$_{PL}$, $P = 0.024$, VIP+$_{PL}$ versus SST+$_{PL}$, $P = 0.012$). In both the PL and ILA areas, PV+ neurons received the smallest input from the substantia innominata (SI) (Fig. 2b, PV+$_{PL}$ versus SST+$_{PL}$, $P = 0.017$, PV+$_{ILA}$ versus VIP+$_{ILA}$, $P = 0.039$). In the amygdala, RV-labeled neurons mainly appeared in the basolateral amygdala (BLA). SST+$_{PL}$ seemed to receive more inputs from the BLA than did PV+$_{PL}$ (Supplementary Fig. 7g); however, the variability across animals prevented this observation from reaching significance ($P = 0.066$). In the thalamus, inputs from the mediodorsal thalamic nucleus to VIP+ neurons were larger than those to SST+ neurons in both the PL and ILA areas (Fig. 2b, VIP+$_{PL}$ versus SST+$_{PL}$, $P = 0.012$; VIP+$_{ILA}$ versus SST+$_{ILA}$, $P = 0.046$). In the hypothalamus, SST+$_{PL}$ received the most inputs from the lateral hypothalamic area (Fig. 2b and Supplementary Fig. 7e, PV+$_{PL}$ versus SST+$_{PL}$, $P = 0.005$; VIP+$_{PL}$ versus SST+$_{PL}$, $P = 0.013$). In the hippocampal formation, ventral hippocampus preferentially innervated SST+$_{PL}$ rather than PV+$_{PL}$ (Fig. 2b and Supplementary Fig. 7h, $P = 0.006$).

As shown in Supplementary Fig. 8, several brain areas also differently innervated the PL and ILA areas. SST+$_{PL}$ received more inputs from the medial orbital cortex ($P = 0.009$), globus pallidus, external part ($P = 0.004$) and ventromedial thalamic nucleus ($P = 0.031$). The lateral septum ($P = 0.001$) and the nucleus of the diagonal band ($P = 0.033$) preferentially innervated SST+$_{ILA}$. The inputs from the ventral tegmental area ($P = 0.047$) and lateral hypothalamic area ($P = 0.034$) to VIP+$_{ILA}$ were larger than those to VIP+$_{PL}$.

Previous studies have shown that both the layer and the topographic location of starter cells dictates input distribution[20–22]. So a major question is to what extent observed differences between cell types were actually dictated by starter-cell location. To address this
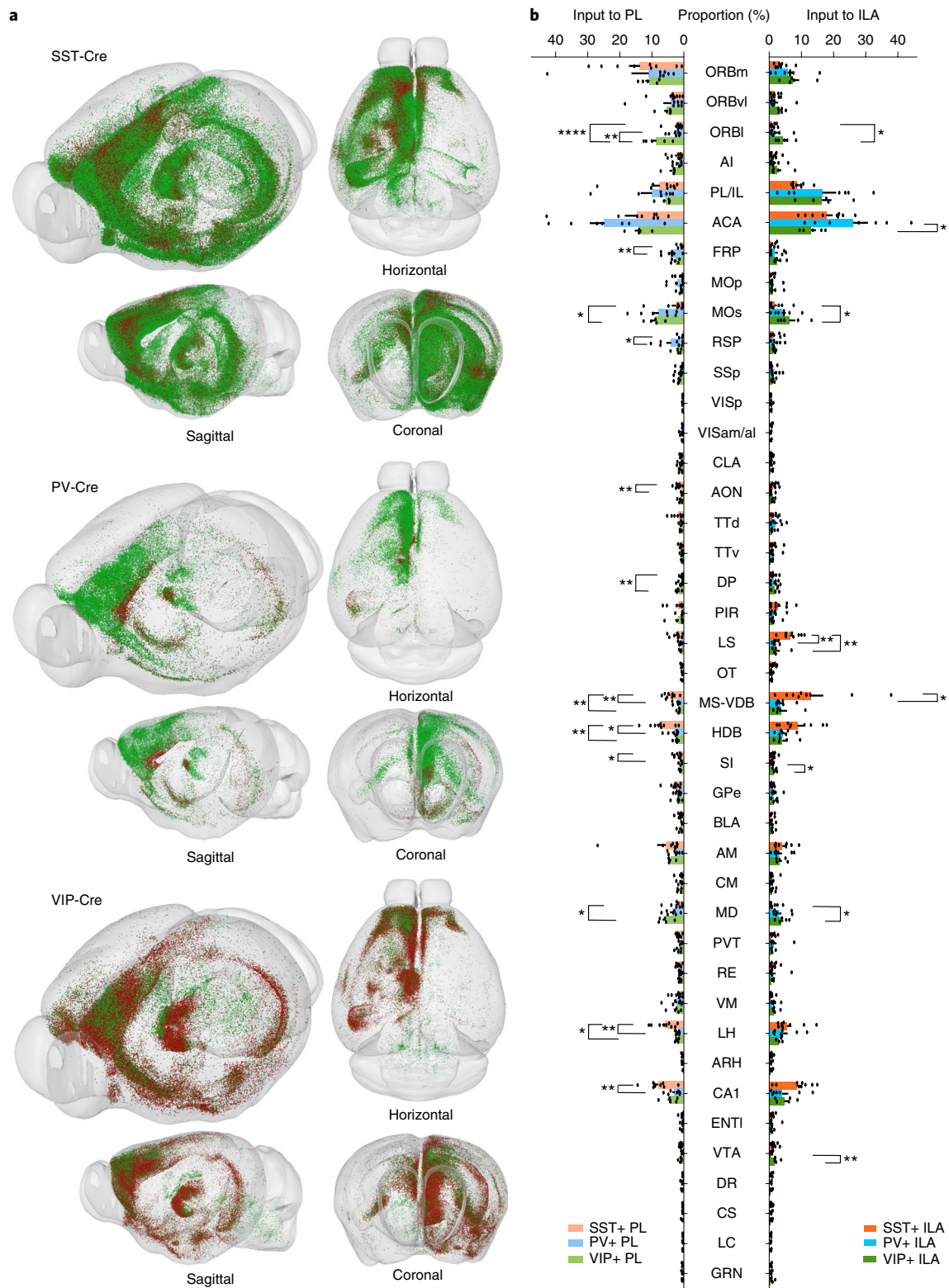
Fig. 2 | Visualization of the whole-brain input neurons to three types of interneurons in two subregions of the mPFC and quantification of the input neurons in individual brain regions. a, AAV helper virus was injected into the PL and ILA areas, RV-EnvA-GFP (green dots) was injected into the PL, and RV-EnvA-DsRed (red dots) was injected into the ILA area. The somas of RV-labeled neurons were extracted by NeuroGPS and registered to the Allen CCF v.3.0. **b**. Proportions of long-range inputs to PV+, SST+ and VIP+ neurons in two subregions of the mPFC across individual brain areas. One-way ANODRVA followed by Tukey's post hoc tests, *$P < 0.05$, **$P < 0.01$, ****$P < 0.0001$; SST+, $n = 18$ mice; PV+, $n = 14$ mice; VIP+, $n = 10$ mice; for detailed P values, see text. Data shown as mean ± s.e.m. See the details in Supplementary Table 4. A list of abbreviations is provided in Supplementary Table 15.

issue, we mapped the three-dimensional (3D) distribution of starter cells along the anterior–posterior (AP) axis (Supplementary Fig. 9a). We also calculated the mean vertical distance of the starter cells

to the midline, brain surface and the coronal plane under bregma point. The starter cells in VIP-Cre mice were closer to the midline than those in PV-Cre and SST-Cre mice (Supplementary Fig. 9b).
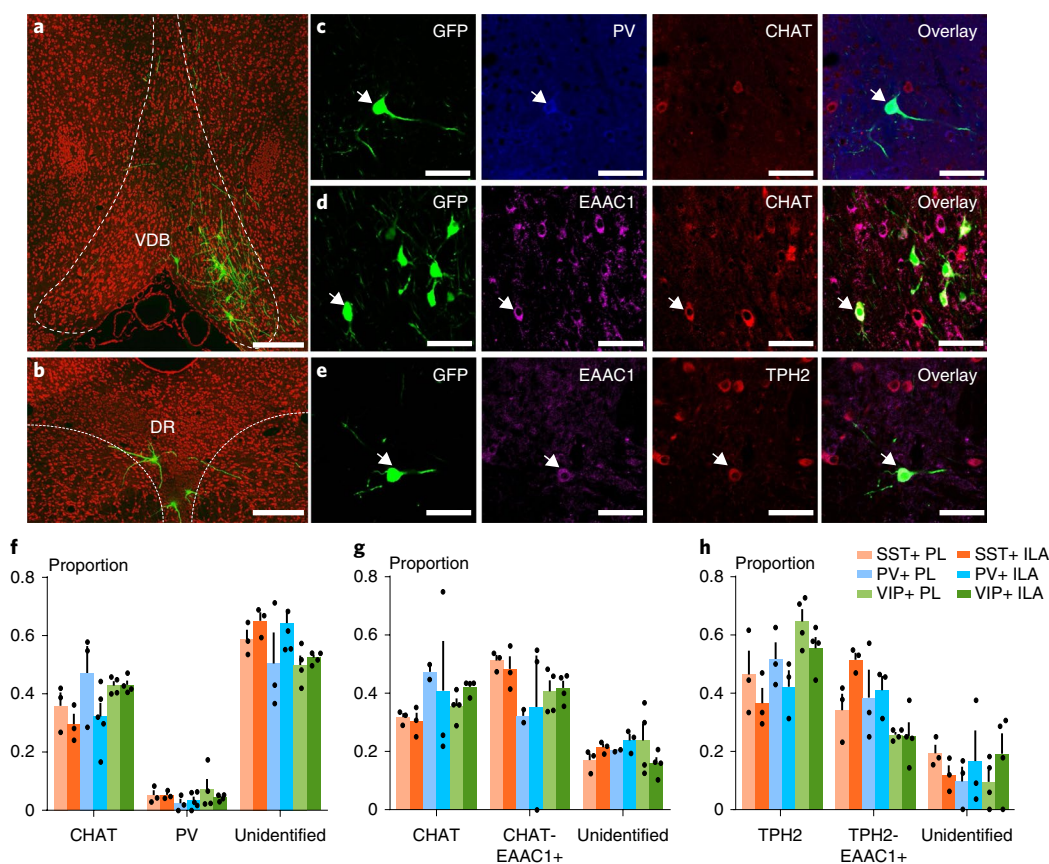
Fig. 3 | Modulation of GABAergic neurons in the mPFC by multiple neurotransmitters. a, GABAergic neurons in the mPFC receive direct inputs from the basal forebrain (SST+, $n=18$ mice; PV+, $n=14$ mice; VIP+, $n=10$ mice). **b**, GABAergic neurons in the mPFC receive direct inputs from raphe nuclei (SST+, $n=18$ mice; PV+, $n=14$ mice; VIP+, $n=10$ mice). **c,d**, Both PV+ neurons and cholinergic neurons in the basal forebrain form monosynaptic inputs to GABAergic neurons in the mPFC, and most of the cholinergic neurons also express EAAC1 (PV and CHAT double immunostaining, SST+, $n=6$ mice; PV+, $n=8$ mice; VIP+, $n=8$ mice; CHAT and EAAC1 double immunostaining, SST+, $n=6$ mice; PV+, $n=5$ mice; VIP+, $n=8$ mice). **e**, Serotonergic neurons in raphe nuclei directly input to GABAergic neurons in the medial cortex, and most of them express EAAC1 (SST+, $n=6$ mice; PV+, $n=6$ mice; VIP+, $n=8$ mice). **f**, Quantification of EGFP-labeled neurons that are cholinergic and PV+ (SST+, $n=6$ mice; PV+, $n=8$ mice; VIP+, $n=8$ mice, data shown as mean $\pm$ s.e.m.). **g**, Quantification of EGFP-labeled neurons that are cholinergic and EAAC1+ (SST+, $n=6$ mice; PV+, $n=5$ mice; VIP+, $n=8$ mice, data shown as mean $\pm$ s.e.m.). **h**, Quantification of EGFP-labeled neurons that are serotonergic and EAAC1+ (SST+, $n=6$ mice; PV+, $n=6$ mice; VIP+, $n=8$ mice, data shown as mean $\pm$ s.e.m.). Scale bars, **a,b**, 200 μm; **c–e**, 50 μm.

We could also clearly see that starter cells in PL-targeting samples and ILA-targeting samples were rather separated (Supplementary Fig. 9a,c,d). To determine the relationship between the spatial distribution of starter cells and input patterns, we performed a linear regression. Consistent with a previous study[22], our results suggested that the spatial distribution of starter cells is an important determinant of input patterns (Supplementary Fig. 9e,f and Supplementary Table 5); however, in the present study, the Cre line is another important determinant of input patterns (Supplementary Fig. 9f and Supplementary Table 5).

Neurochemical characterization of the subcortical input neurons. To characterize the neurochemical properties of the input neurons, we employed double immunochemical staining against several biological markers. GABAergic neurons in the mPFC express acetylcholine and serotonin receptors and can be activated by acetylcholine and serotonin[23,24]. We found that RV-labeled input neurons were distributed in several brain areas, including the basal forebrain, ventral tegmental area and raphe nuclei (Fig. 3a,b and Supplementary Fig. 10). All three types of GABAergic neurons in the mPFC were directly innervated by PV+ projection neurons, cholinergic neurons in the basal forebrain and serotonergic neurons in raphe nuclei (Fig. 3c–e and

Supplementary Fig. 10a,c). These PV+ projection neurons did not express choline acetyltransferase (Fig. 3c) and were only a small part (5%) of input neurons in the basal forebrain (Fig. 3f and Supplementary Table 6).

Approximately 30–40% of the input neurons in the basal forebrain were cholinergic (Fig. 3g, Supplementary Fig. 10a and Supplementary Table 6), consistent with previous studies[25]. Over 80% of these cholinergic neurons also expressed glutamate transporter EAAC1 (ref. [26]; Fig. 3d and Supplementary Fig. 10h). Less than 20% of these cholinergic neurons expressed choline acetyltransferase alone (Supplementary Fig. 10a,h), while approximately 50% of the input neurons in the basal forebrain expressed EAAC1 alone (Fig. 3g, Supplementary Fig. 10b and Supplementary Table 6). These data showed that SST+ neurons in the mPFC received more inputs from the basal forebrain than did PV+ neurons (Fig. 2b), indicating that the SST+ $_{mPFC}$ receive more modulation from cholinergic neurons in the basal forebrain.

In raphe nuclei, approximately half of the RV-labeled neurons expressed tryptophan hydroxylase, the biomarker for serotoninergic neurons (Fig. 3h). More than 70% of these serotoninergic input neurons also expressed EAAC1 (Fig. 3e, Supplementary Fig. 10i), consistent with a recent study[27]. Approximately 40% of the input
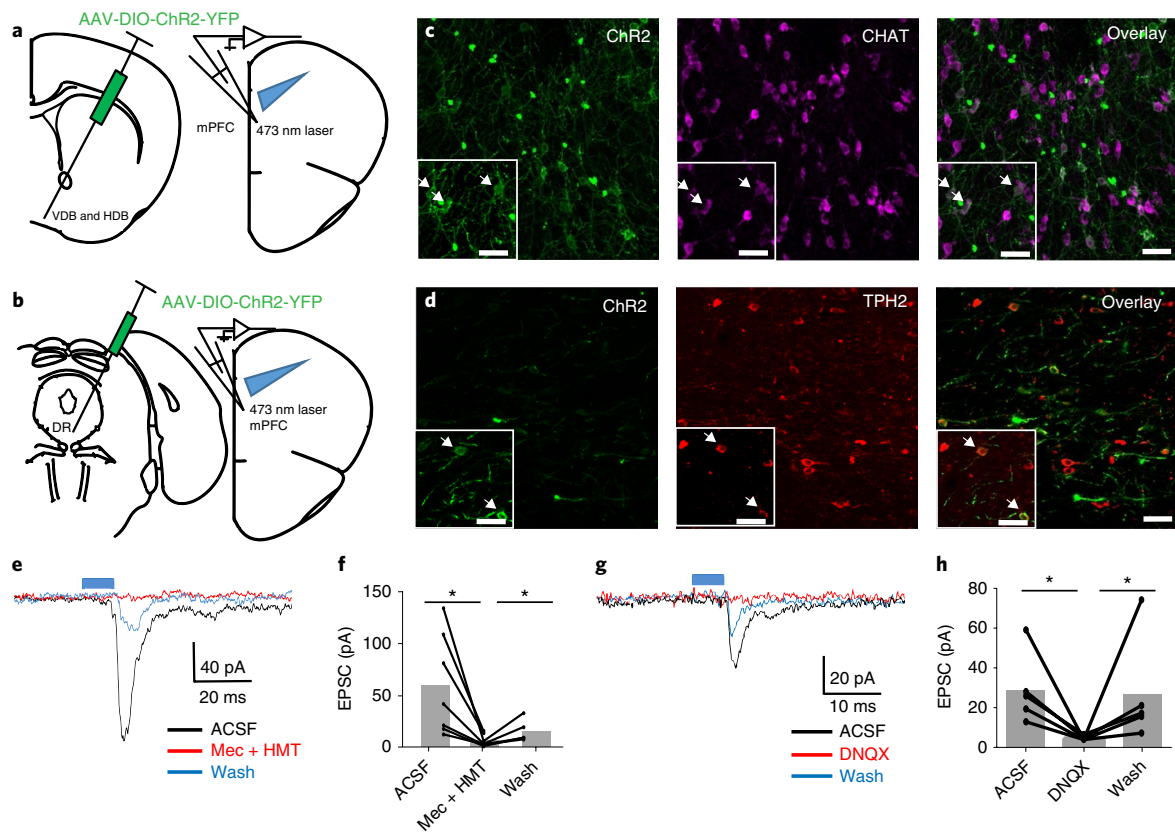
Fig. 4 | Characterization of the functional inputs from cholinergic neurons in basal forebrain and serotonin neurons in raphe nuclei to GABAergic neurons in the mPFC. a, Experimental designs for recordings of GABAergic neurons in the mPFC following AAV-DIO-ChR2 injections in VDB and HDB of chat-Cre:GAD67-GFP mice. **b**, Experimental designs for recordings of GABAergic neurons in the mPFC following AAV-DIO-ChR2 injections in raphe nuclei of sert-Cre:GAD67-GFP mice. **c,d**, Immunostaining against CHAT and TPH2, respectively, to validate the specificity of ChR2 expression. Enlarged images are given in the boxes in **c** and **d** (chat-Cre:GAD67-GFP, $n = 6$ mice; sert-Cre:GAD67-GFP, $n = 6$ mice). **e**, Example traces of GABAergic neuron recordings with paired-pulse laser-evoked stimulation of cholinergic terminals in the mPFC. The EPSCs can be blocked by Mec + MHT (7 of 34 cells in 6 mice). **f**, Effects of Mec and HMT on EPSCs evoked by blue-light stimulation of chat + fibers when recording GABAergic neurons in the mPFC (7 cells in 6 mice, two-tailed paired t-test, *$P < 0.05$, aCSF versus Mec + HMT, $P = 0.014$, Mec + HMT versus Wash, $P = 0.038$). **g**, Example traces of GABAergic neuron recordings with paired-pulse laser-evoked stimulation of cholinergic terminals or serotoninergic terminals in the mPFC. The EPSCs can be blocked by DNQX (2 of 34 cells in 6 Chat-Cre:GAD67-GFP mice, 3 of 63 cells in 6 sert-Cre:GAD67-GFP mice). **h**, Effect of DNQX on EPSCs evoked by blue-light stimulation of chat fibers or 5-hydroxytryptamine fibers when recording GABAergic neurons in the mPFC (5 cells in 6 mice). Scale bars, **c,d**, 50 μm (two-tailed paired t-test, *$P < 0.05$, ACSF versus DNQX, $P = 0.038$, DNQX versus Wash, $P = 0.019$). aCSF, artificial cerebrospinal fluid; wash, antagonists are washed out with aCSF.

neurons in the raphe nuclei expressed EAAC1 alone (Fig. 3h, Supplementary Fig. 10d and Supplementary Table 6).

To examine whether cholinergic neurons and serotoninergic neurons can release other neural transmitters as previously reported[28,29], we performed optogenetic-assisted circuit mapping to assess the functional connectivity among cholinergic neurons, serotoninergic neurons and GABAergic neurons in the mPFC. Briefly, the chat-Cre or sert-Cre driver lines were crossed with the GAD67-GFP line[30] to label GABAergic neurons in the mPFC. A Cre-dependent AAV that expressed channelrhodopsin (ChR2) was injected into the VDB and HDB of chat-Cre mice or the raphe nuclei of sert-Cre mice (Fig. 4a,b). The ChR2 was strictly expressed in cholinergic neurons or serotoninergic neurons (Fig. 4c,d). We subsequently performed whole-cell recordings paired with blue-light stimulation on GABAergic neurons in the mPFC. A single train of light stimulation could elicit fast-latency excitatory postsynaptic currents (EPSCs) in GABAergic neurons in the mPFC. These EPSCs could be completely blocked by the ACh receptor (nAChR) antagonist Mec and the mACHR antagonist HMT (Fig. 4e,f and Supplementary Table 7). The result indicated that cholinergic neurons of the basal forebrain activated GABAergic neurons in the mPFC by ACh. Surprisingly, some EPSCs elicited by stimulating cholinergic fibers were blocked

by the AMPA antagonist DNQX (Fig. 4g, h and Supplementary Table 7), indicating that cholinergic axons also released glutamate to activate GABAergic neurons in the mPFC. We repeated this experimental procedure in sert-Cre:GAD67-GFP mice and found that a single train of light stimulation could also elicit fast-latency EPSCs in GABAergic neurons in the mPFC. These EPSCs could be blocked by the AMPA antagonist DNQX (Fig. 4g, h and Supplementary Table 7), indicating that serotoninergic neurons could release glutamate onto GABAergic neurons in the mPFC. These patch results confirmed that cholinergic neurons in the basal forebrain and serotoninergic neurons in the raphe nuclei can release glutamate to activate GABAergic neurons in the mPFC.

Although it is known that $PV+_{mPFC}$ can be directly modulated by dopaminergic neurons in the VTA[11], we found that only a small part (approximately 5%) of the VTA neurons that project to $PV+_{mPFC}$ and $VIP+_{mPFC}$ were dopaminergic; however, no dopaminergic VTA neurons directly projected to $SST+_{mPFC}$ (Supplementary Fig. 10e–g and Supplementary Table 6).

Neural circuits among the SI, anteromedial thalamic nucleus and mPFC. To certify the organization pattern of input neurons, we analyzed the upstream circuits in precise whole-brain data

sets. The results showed that neurons in the SI and anteromedial thalamic nucleus (AM) could directly project to three types of GABAergic neurons in the mPFC (Fig. 2b and Fig. 5a,b). In a 3D view, neurons in the SI clearly sent enormous axon arbors to the mPFC and the AM, which itself also generated dense projections to the mPFC (Fig. 5b). Reconstructing the morphology of the neurons in the SI that project to the mPFC showed that some of these neurons indeed generated collateral projections to the AM (Fig. 5c). We wondered whether neurons in the SI that project to the mPFC could form synaptic connections with neurons in the AM that target mPFC. First, to confirm that the neurons in the AM that project to the mPFC receive direct inputs from the SI, we employed cTRIO (cell-type-specifically tracing the relationship between input and output) technology[31]. Briefly, we injected CAV-Cre into the mPFC of C57 mice and Cre-dependent AAV helper virus into the AM. After 3 weeks, we injected SAD-ΔG-DsRed(EnvA)-RV into the mPFC (Fig. 5d,e). There were RV-labeled neurons in the SI (Fig. 5f). Unexpectedly, we found that the AM also received direct inputs from the dorsal striatum (Fig. 5g and Supplementary Fig. 11).

To confirm that neurons in the SI project to the mPFC and simultaneously form synaptic connections with the AM that itself projects to the mPFC, we applied cTRIO technology and injected CAV-Cre into the mPFC of Ai14 mice; Cre-dependent AAV helper virus was simultaneously injected into the AM (Fig. 5h). After 3 weeks, SAD-ΔG-GFP(EnvA)-RV was also injected into the AM (Fig. 5h). In the SI, we found three types of neurons: those labeled by GFP, labeled by tdTomato and dual-color labeled by GFP and tdTomato, respectively (Fig. 5i, j and Supplementary Fig. 12a,b). This indicated that these neurons could send their axons to the mPFC and directly connected with neurons in the AM that project to the mPFC. About 18% of the labeled neurons were dual-color labeled (Supplementary Fig. 12c and Supplementary Table 8). Immunohistochemical staining against choline acetyltransferase showed that about 70% of dual-color-labeled neurons were choline acetyltransferase negative and 30% were choline acetyltransferase-positive (Fig. 5j, Supplementary Fig. 12a,b d and Supplementary Table 8).

Moreover, we found that several brain areas, such as the limbic cortex, secondary motor cortex, associative cortex, basal forebrain, several thalamic nuclei, lateral hypothalamic area, hippocampus and several midbrain nuclei, could project to these two areas simultaneously (Fig. 5k,l, Supplementary Fig. 11 and Supplementary Table 9). The AM also received inputs from several brain areas that do not project to the mPFC, such as the reticular thalamic nucleus, the substantia nigra/reticular part and the mammillary nuclei (Fig. 5l). In most brain areas, such as the MOs, HDB, LHA and CA1, distinct neurons innervated mPFC and AM (Fig. 5k, Supplementary Fig. 12e–h and Supplementary Table 8). Based on our viral tracing results, we updated the circuit connectivity among mPFC, SI and AM, as shown in Fig. 5m. We found three types of neurons in the SI based on their projection targets, as well as a dorsal striatum–AM–mPFC circuit.

Classification of individual cortical input neurons. As the major upstream area of GABAergic neurons in the mPFC (Fig. 2b and Supplementary Fig. 6), the cortex contains input neurons with the most varied distribution and morphology. Many cortical neurons in the limbic cortex, motor cortex, sensory cortex and associative cortex projected to PV+, SST+ and VIP+ neurons in the mPFC (Fig. 6a,b). The limbic cortex contained the most cortical input neurons (Fig. 6c). Most of these neurons were located in layers II and III, some in layer V and only a few neurons in layer VI (Fig. 6d). The layer distribution of the cortical input neurons was region dependent; input neurons in the limbic cortex, motor cortex and associative cortex mainly were located in layers II and III, whereas input neurons in the sensory cortex were mainly located in layer V (Fig. 6e–g). The distribution of cortical input neurons in each individual cortical area is plotted in Fig. 6h (also refer to Supplementary Table 10).

To better understand how long-range cortical input neurons control different GABAergic neurons in the mPFC, we reconstructed the fine morphology of single cortical input neurons in different layers of the neocortex to characterize their axonal and dendritic arborizations (Fig. 7a,b). Eighty-six cortical input neurons were reconstructed at different layers of the different cortical areas (Fig. 7c,d and Supplementary Table 11). Cortical neurons in layers II and III that project to the mPFC had typical broad-tufted dendrites and their axons projected to the ipsilateral cortex, ipsilateral striatum and contralateral cortex (Fig. 7e,f, Supplementary Fig. 13 and Supplementary Table 11).

Cortical input neurons in layer Va comprise at least three types that project to GABAergic neurons in the mPFC: callosal pyramidal neurons, associative pyramidal neurons and stellate cells. Callosal pyramidal neurons had sparse apical dendrites, and their axons could project to the ipsilateral cortex, ipsilateral striatum, entorhinal cortex, contralateral cortex and contralateral striatum (Fig. 7e,f, Supplementary Fig. 13 and Supplementary Table 11). Associative pyramidal neurons also had slender apical dendrites but more apical dendritic branches (Fig. 7f). This type of neuron could send its axons to the ipsilateral striatum but not the contralateral cortex (Fig. 7e, Supplementary Fig. 13 and Supplementary Table 11). The callosal pyramidal neurons and associative pyramidal neurons that target GABAergic neurons in the mPFC have similar dendritic morphologies to cortical neurons previously described as tall simple layer V pyramidal neurons[32]. The stellate cells did not have apical dendrites (Fig. 7f). Their axons could project to the contralateral cortex (Fig. 7e, Supplementary Fig. 13 and Supplementary Table 11). This type of neuron has a similar morphology to the recently reported callosal PV+ neurons in the cortex[33]. Moreover, this type of neuron was only observed in SST-Cre mice but not in PV-Cre mice or VIP-Cre mice when monosynaptic tracing was performed in the mPFC (Supplementary Fig. 13).

We also found two types of cortical input neurons in layer Vb that project to GABAergic neurons in the mPFC: corticofugal non-spinal cord projection pyramidal neurons and corticospinal

Fig. 5 | A neural circuit among mPFC, SI and AM. a, Labeling direct input neurons in AM and SI to different GABAergic neurons in the mPFC with monosynaptic RV tracing. **b**, 3D view of the RV-labeled somas and axons in SI and AM. The boxed image in **b** shows a neuron in the AM and axons from SI (SST+, n = 18 mice; PV+, n = 14 mice; VIP+, n = 10 mice). The arrowhead indicates the axon terminals. **c**, The morphology of neurons in SI that innervated mPFC and AM (n = 2 mice). **d**, Labeling direct inputs to neurons in AM that project to the mPFC using the cTRIO strategy. **e**, The starter cells (yellow) and local input neurons (red) at the RV injection site; n = 6 mice. **f,g**, Neurons in SI and CPu can directly project to neurons in AM that project to the mPFC, n = 6 mice. **h**, Strategy for labeling neurons that directly project to the mPFC and indirectly project to the mPFC through AM. **i,j**, Neurons in SI can directly project to the mPFC and send collateral projections to neurons in AM that project to the mPFC, and a non-cholinergic neuron labeled by GFP and tdTomato is shown in **j** (n = 4 mice). **k**, Within MOs, HDB, LHA and CA1, distinct neurons project to the mPFC and AM (MOs, HDB, n = 4 mice; LHA, CA1, n = 3 mice). **l**, Quantification of inputs to neurons in AM that project to the mPFC, n = 6 mice, data shown as mean ± s.e.m. **m**, An updated circuitry model among the mPFC, SI and AM. The conventional circuits are shown in black and the circuits revealed in this study are shown in other colors. Scale bar, boxed image in **b**, 20 μm; **i**, 1 mm; **e–g,k**, 100 μm; **j**, 50 μm. CA1, CA1 area of the hippocampus; CPu, caudoputamen; MO, motor area; LHA, lateral hypothalamic area; L, left; R, right; D, dorsal; V, ventral.

pyramidal neurons. The two types of neurons shared similar patterns of dendritic arborization, which are consistent with tall tufted layer V pyramidal neurons in previous studies[32] (Fig. 7f); however, their axons targeted different brain areas. They both had tufted apical dendrites and enormous oblique side branches; one type of neuron could send their axons to the tegmental areas and pons but not the medulla (Fig. 7e, Supplementary Fig. 13, and Supplementary

Table 11), while the other type of neurons could send their axons to the medulla and spinal cord (Fig. 7e, Supplementary Fig. 13 and Supplementary Table 11). The latter was only observed in PV-Cre mice and not in SST-Cre mice or VIP-Cre mice (Supplementary Fig. 13). The corticospinal pyramidal neurons found in the present study have similar morphology and projection patterns to the medulla projecting neurons described in a recent report[34].
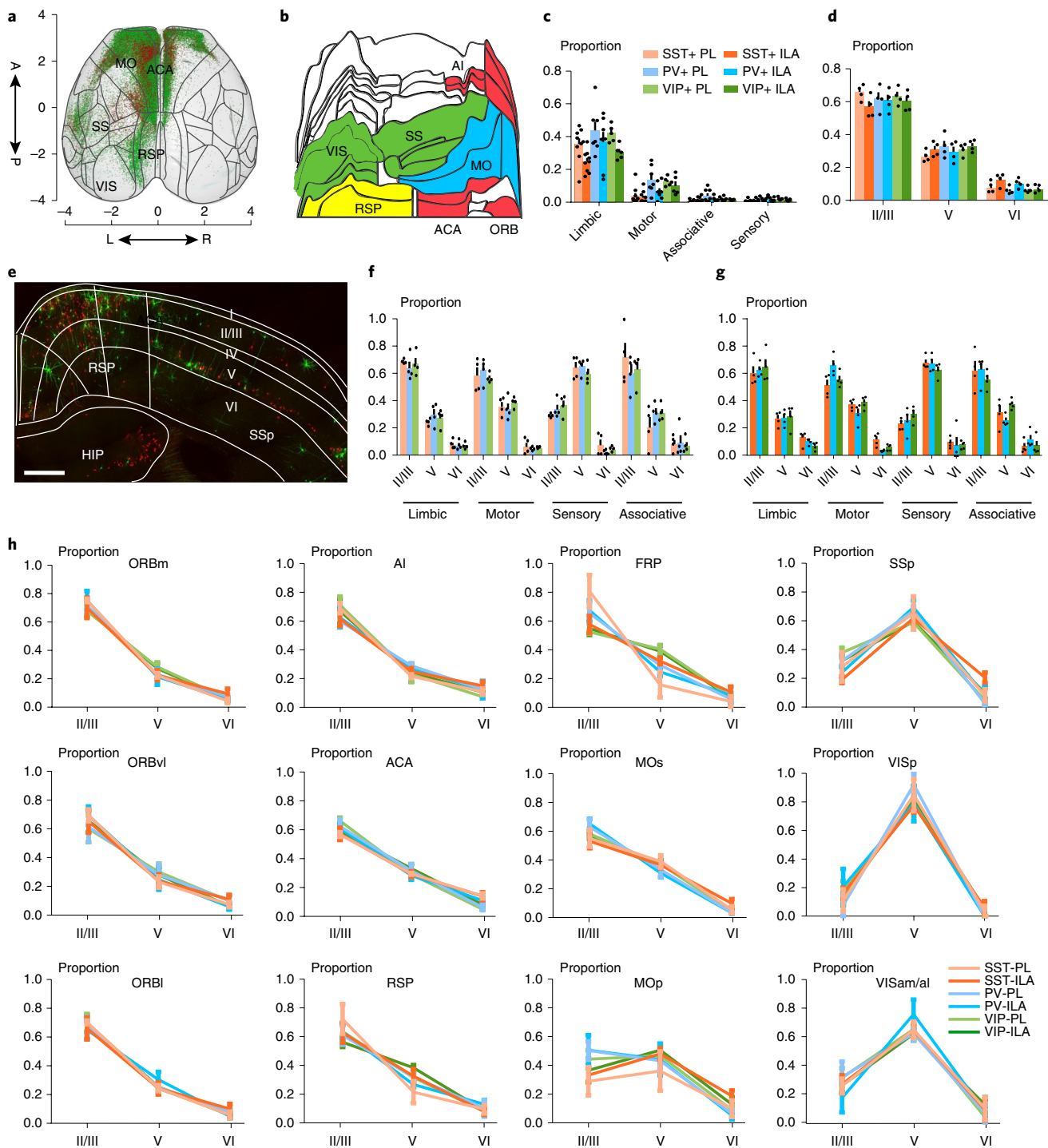

Circuits between mPFC, AM and SI
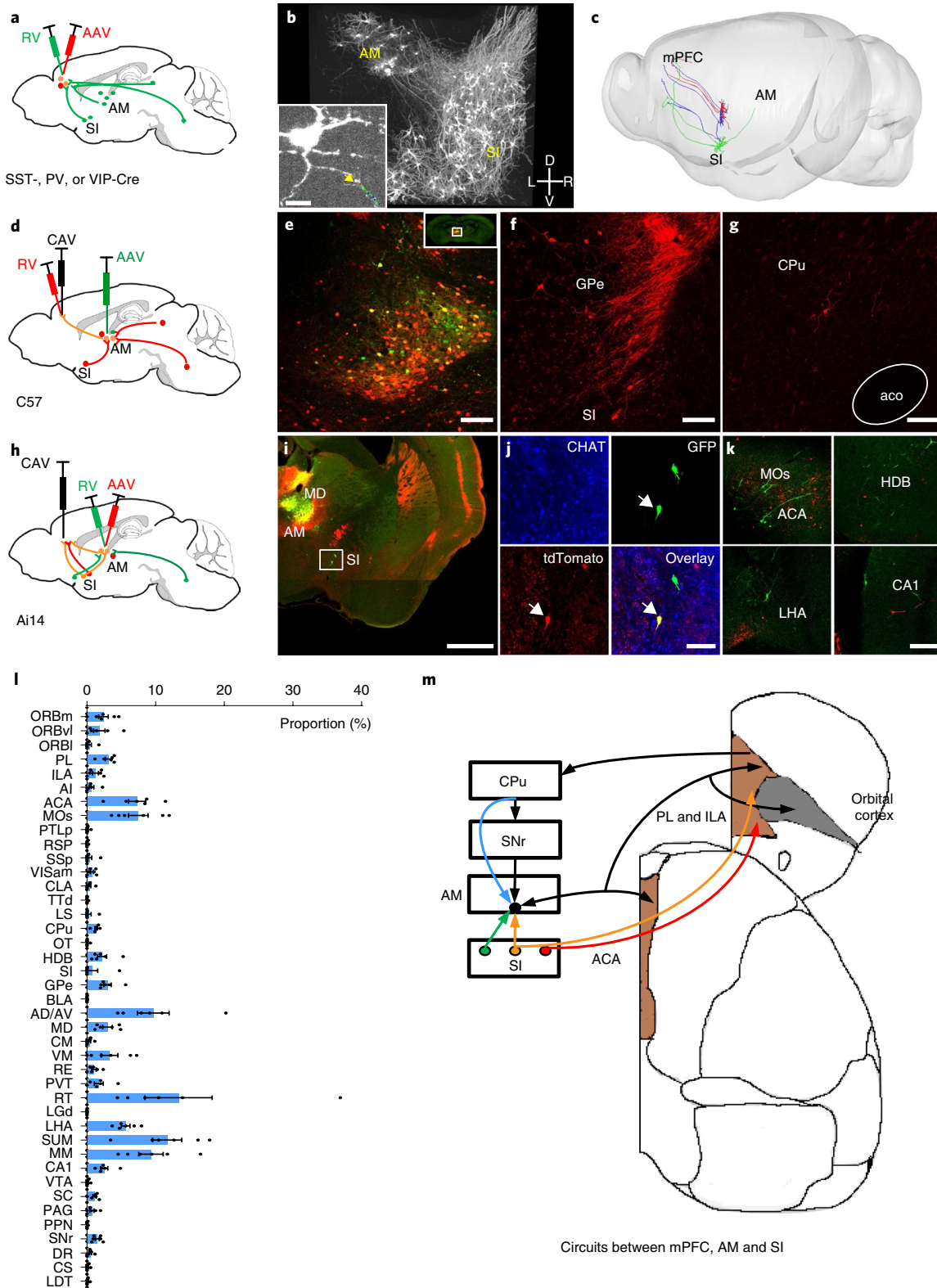
Fig. 6 | Distribution of input neurons in the neocortex to three types of GABAergic neurons in the mPFC. a, The distribution of cortical input neurons in different cortical regions in a horizontal view. **b**, The flattened view of the mouse cortex in the reference atlas showed the anatomical locations of the input neurons in different cortical areas that target GABAergic neurons in the mPFC. The limbic cortex includes the orbital cortex, agranular insular cortex and cingulate cortex. The motor cortex consists of the frontal association cortex, secondary motor cortex and primary motor cortex. The primary somatosensory cortex, primary visual cortex and secondary visual cortex comprise the sensory cortex. The associative cortex mainly includes the retrosplenial granular cortex. The limbic areas are shown in red, the motor areas are shown in blue, the sensory areas are shown in green and the associative areas are shown in yellow. **c**, Cortical input neurons were mainly located in the limbic areas of the cortex (SST+, $n=18$ mice; PV+, $n=14$ mice; VIP+, $n=10$ mice, data shown as mean±s.e.m.). **d**, Cortical input neurons were mainly located in layers II/III of the cortex (SST+, $n=8$ mice; PV+, $n=8$ mice; VIP+, $n=8$ mice, data shown as mean±s.e.m.). **e**, The distribution of cortical input neurons in RSP and SSp. There are differences in the layer distribution of cortical input neurons between RSP and SSp (SST+, $n=18$ mice; PV+, $n=14$ mice; VIP+, $n=10$ mice). **f,g**, Quantification of cortical input neurons to the PL (**f**) and ILA (**g**) areas in grouped cortical areas (SST+, $n=8$ mice; PV+, $n=8$ mice; VIP+, $n=8$ mice, data shown as mean±s.e.m.). The cortical input neurons in the limbic cortex, motor cortex and associative cortex were mainly located in layers II/III, while the cortical input neurons in the sensory cortex were mainly located in layer V. **h**, Quantification of cortical input neurons to the PL and ILA areas in each individual cortical area (SST+, $n=8$ mice; PV+, $n=8$ mice; VIP+, $n=8$ mice, data shown as mean±s.e.m.). Scale bar, **e**, 500 μm. A, anterior; P, posterior; L, left; R, right; RSP, retrosplenial area; SSp, primary somatosensory area.

In layer VI, we found that a few cortical neurons could also project to GABAergic neurons in the mPFC. This type of neuron had very short apical dendrites, which terminated at layer V (Fig. 7f), resembling the small cortical neuron in previous reports[35]. Their axons projected to the contralateral cortex (Fig. 7e, Supplementary Fig. 13 and Supplementary Table 11).

To certify the morphological differences among different layer V pyramidal neurons, we quantified the dendritic morphology of four different pyramidal neurons in layer V. Among the four types of pyramidal neurons, the corticospinal pyramidal neurons possessed the most dendritic branches and dendritic length, while the callosal pyramidal neurons possessed the least dendritic branches and dendritic length (Fig. 7g, Supplementary Fig. 14a and Supplementary Table 12). Compared with the callosal pyramidal neurons, the associative neurons possessed more apical dendritic branches and apical dendritic length (Fig. 7h, Supplementary Fig. 14b and Supplementary Table 12). Finally, we identified seven different types of cortical neurons in the neocortex projecting to GABAergic neurons in the mPFC with different axonal and dendritic arborizations (Fig. 7i).

Input from hippocampal neurons. The hippocampal formation is another major area that regulates the activity of the mPFC[36,37]. To verify the heterogeneity of hippocampal input neurons that target different GABAergic neurons in the mPFC, we reconstructed the morphology of 33 hippocampal pyramidal neurons. We found that SST+, PV+ and VIP+ neurons in the mPFC received direct inputs from hippocampal pyramidal neurons (Fig. 8a–c). Hippocampal pyramidal neurons are more heterogeneous than previously thought[38]. Indeed, we found that some hippocampal pyramidal neurons that target different GABAergic neurons had unique axon collateral projections (Fig. 8d). Some hippocampal pyramidal neurons that target SST+ neurons in the mPFC could also project to the contralateral CA1, while the hippocampal pyramidal neurons that target PV+ neurons in the mPFC tended to send their collateral projections to the accumbens nucleus (ACB). To confirm this projection bias, we performed double RV labeling. Briefly, the Cre-dependent AAV helper virus was injected into the mPFC of SST-Cre, PV-Cre or VIP-Cre mice. After 3 weeks, the EnvA-coated RV expressing GFP and the RG-coated RV expressing DsRed were injected into the mPFC and ACB, respectively (Fig. 8e–g). After 10 days, we found GFP-labeled pyramidal neurons (mPFC projecting), DsRed-labeled pyramidal neurons (ACB projecting) and dual-color-labeled pyramidal neurons (double projecting) in the hippocampus (Fig. 8h). However, in PV-Cre mice, approximately 15% of the GFP-labeled pyramidal neurons were colocalized with the DsRed-labeled pyramidal neurons, while in VIP-Cre mice only 5% of the GFP-labeled pyramidal neurons were colocalized with the DsRed-labeled pyramidal neurons (Fig. 8i, $P < 0.001$, and Supplementary Table 13). Thus, based on our tracing and double

RV-labeling results, we designed a model of hippocampal pyramidal neurons regulating GABAergic neurons in the mPFC (Fig. 8j): most of the hippocampal pyramidal neurons that target GABAergic neurons have similar a projection pattern, but a few have unique axon projections.

Discussion

In the present study, we employed RV-tracing and whole-brain precise imaging to obtain a comprehensive atlas of the long-range inputs to PV+, SST+ and VIP+ neurons in the mPFC. We demonstrated that the upstream brain areas that project to different subtypes of interneurons in both subregions of the mPFC are similar but with quantitative differences. To characterize the input neurons and input circuits, we studied the neurochemical properties of the subcortical input neurons and the morphology of cortical and hippocampal input neurons. Notably, by combining whole-brain precise imaging with state-of-the-art viral genetic tools, we identified different types of cortical and hippocampal neurons and novel neural circuits among the mPFC and the upstream input brain areas.

Monosynaptic inputs of PV+, SST+ and VIP+ neurons in the mPFC. Consistent with a previous study[7], we found that PV+, SST+ and VIP+ neurons in both subregions of the mPFC receive inputs from similar brain areas. However, the PL and ILA area were innervated by different neurons in these brain areas (Supplementary Figs. 4 and 5). Previous studies demonstrated that PL-innervating and ILA-innervating neurons in BLA have different molecular markers and functions[16]. It is possible that this is also the case for neurons in the other brain areas identified here.

There are also several differences among the long-range input patterns of different subtypes of GABAergic neuron. SST+ neurons receive the least inputs from the cortex, while some subcortical areas preferentially innervate SST+ neurons in the mPFC, such as the lateral septum, diagonal band, lateral hypothalamic area and CA1, which are known to be involved in hippocampal–PFC circuitry[39]. These biased inputs suggest that SST+ neurons in the mPFC may play a key role in the hippocampal–PFC circuitry[40].

The most significant difference between the input patterns of PV+ and VIP+ neurons is that PV+ neurons receive more inputs from the cingulate cortex (involved in decision-making and goal-directed actions), while VIP+ neurons receive more inputs from the lateral orbital cortex (involved in processing sensory stimuli[41]). This suggests that PV+ neurons and VIP+ neurons in the mPFC may process cognitive and sensory receiving functions, respectively.

Previous studies have demonstrated that the spatial distribution of starter cells can greatly affect the input patterns[20–22]. Our results also showed that the spatial distribution of starter cells is an important determinant to the input patterns (Supplementary Fig. 9). However, the Cre lines also contributed to the input patterns (Supplementary Fig. 9), possibly because in the VTA (investigated

Fig. 7 | Characterization of the morphological properties of the cortical neurons that directly input to GABAergic neurons in the mPFC. a, GABAergic neurons in the mPFC receive inputs from other cortical areas. **b**, Enlarged image of boxed area in **a** showing the input cortical neurons in layers II/III and V (SST+, $n = 18$ mice; PV+, $n = 14$ mice; VIP+, $n = 10$ mice). **c**, Eighty-six traced neurons were registered to the Allen CCF v.3.0. Neurons in layers II/III are shown in red, neurons in layer V are shown in blue, and neurons in layer VI are shown in green. **d**, Neurons that target SST+, PV+ and VIP+ neurons are shown in different brain frameworks. **e**, Seven different types of cortical neurons that target GABAergic neurons in the mPFC. **f**, The dendritic morphologies of seven different types of cortical neurons that target GABAergic neurons in the mPFC. Layer II/III neurons are shown in red. Layer V associative neurons, callosal neurons, corticofugal non-SP neurons, corticospinal neurons and stellate neurons are shown in blue, while layer VI neurons are shown in green. **g,h**, Quantitative comparison of the fine morphology of four types of different pyramidal neurons in layer V that target GABAergic neurons in the mPFC. Histograms of the dendrite branch numbers (**g**) and the apical dendrite branch numbers (**h**) (**g**, one-way ANOVA followed by Tukey's post hoc tests, callosal neurons, $n = 19$, associative neurons, $n = 16$, corticofugal neurons, $n = 17$, corticospinal neurons, $n = 5$, **$P < 0.01$, ***$P < 0.001$, ****$P < 0.0001$, callosal neurons versus corticofugal neurons, $P = 0.0016$, callosal neurons versus corticospinal neurons, $P < 0.0001$, corticofugal neurons versus corticospinal neurons, $P = 0.0007$, corticospinal neurons versus associative neurons, $P < 0.0001$, data shown as mean ± s.e.m.; **h**, callosal neurons, $n = 19$, associative neurons, $n = 16$, two-tailed unpaired t-test, $P = 0.0042$, data shown as mean ± s.e.m.). **i**, A model of different cortical neuron inputs to GABAergic neurons in the mPFC. Scale bar, **a**, 500 μm; **b**, 100 μm. CON, contralateral; A, anterior; P, posterior; M, medial; L, lateral; D, dorsal; V, ventral.

in ref. [22]) neurons with different biomarkers largely overlap, whereas this is not the case for PV+, SST+ and VIP+ neurons in the cortex.

Neurochemical properties of subcortical inputs. The release mechanisms of acetylcholine and serotonin in the cortex have been a long-lasting point of dispute[42]. The release of 5-hydroxytryptamine and glutamate by serotoninergic neurons that project to the

VTA and ACB has been reported[29], and serotoninergic terminals in the mPFC express vglut2 (ref. [43]). The release of glutamate by cholinergic neurons of the basal forebrain has been demonstrated in cultured neurons[44]. Our results showed that cholinergic neurons in the basal forebrain and serotoninergic neurons in raphe nuclei that project to the mPFC express excitatory amino acid carrier 1 and release glutamate to activate GABAergic neurons in the mPFC
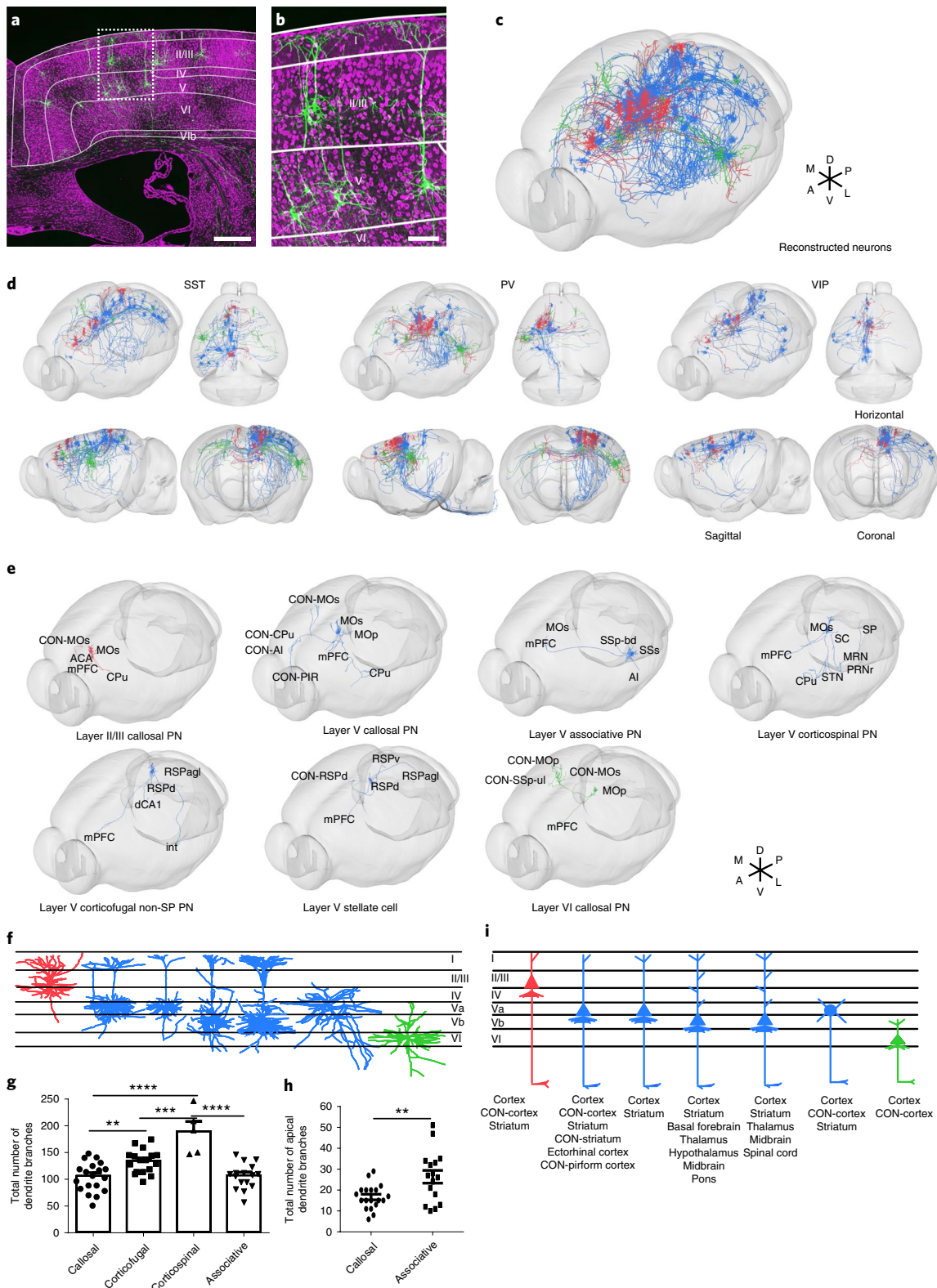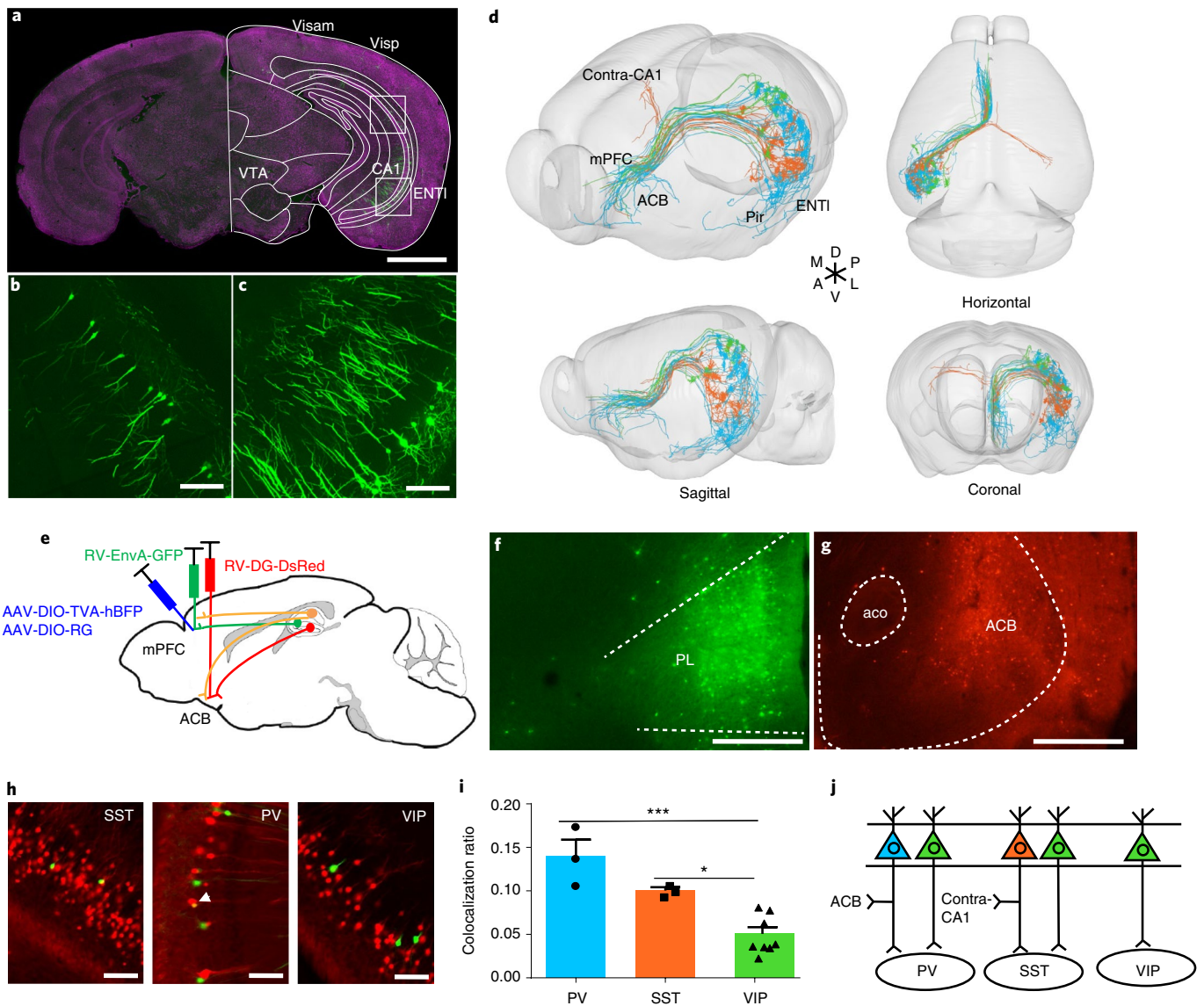
Fig. 8 | Characterization of the morphological properties of the hippocampal pyramidal neurons that directly input to GABAergic neurons in the mPFC. a, A 50-μm projection image showing input cells in the hippocampus and midbrain. **b,c**, Enlarged images of the boxed areas in **a** (SST+, $n = 18$ mice; PV+, $n = 14$ mice; VIP+, $n = 10$ mice). **d**, Thirty-three traced hippocampal pyramidal neurons that target GABAergic neurons in the mPFC. Neurons targeting SST+ neurons in the mPFC are shown in orange, neurons targeting PV+ neurons in the mPFC are shown in blue, and neurons targeting VIP+ neurons in the mPFC are shown in green. Neurons targeting SST+ neurons in the mPFC can send collateral projections to the contralateral CA1 region, while neurons targeting PV+ neurons in the mPFC can simultaneously project to the ACB. **e**, The strategy for labeling hippocampal pyramidal neurons that simultaneously target GABAergic neurons in the mPFC and ACB. **f,g**, The injection sites of the PL area and ACB. **h**, The neurons in the hippocampus that target GABAergic neurons in the mPFC are labeled by GFP, and the neurons in the hippocampus that project to the ACB are labeled by DsRed. The arrowhead shows the dual-color-labeled neurons in the hippocampus (SST+, $n = 3$ mice; PV+, $n = 3$ mice; VIP+, $n = 8$ mice). **i**, Neurons in the hippocampus that target PV+ neurons in the mPFC tend to project to the ACB simultaneously (one-way ANOVA followed by Tukey's post hoc tests, *$P < 0.05$, ***$P < 0.001$, SST+, $n = 3$ mice; PV+, $n = 3$ mice; VIP+, $n = 8$ mice, PV+ versus VIP+, $P = 0.0003$, SST+ versus VIP+, $P = 0.025$, data shown as mean ± s.e.m.) **j**, A model of hippocampal pyramidal neurons targeting different GABAergic neurons in the mPFC. Scale bars, **a**,**f**,**g**, 1 mm; **b**,**c**,**h**, 100 μm.

(Figs. 3 and 4). The direct inputs from PV+ neurons in the basal forebrain to PV+$_{mPFC}$ have been shown to be related to the modulation of gama oscillations[10] and the exact role of the connectivity of PV+$_{basal\ forebrain}$→SST+$_{mPFC}$ or PV+$_{basal\ forebrain}$ → VIP+$_{mPFC}$ must be further investigated.

More cholinergic inputs to SST+ neurons in the mPFC imply that acetylcholine release may preferentially drive SST inhibition. However, there was no difference in serotoninergic inputs between different cell types or subregions, which indicates cholinergic neurons modulate in a modality-specific manner and serotoninergic neurons modulate in a divergent manner[45].

Neural circuits between mPFC and upstream input areas. In this study we identified several neural connections that, to our knowledge, have not been reported previously. First, both cholinergic and non-cholinergic neurons in the SI can project to the mPFC and simultaneously form synaptic connections with neurons in the AM that project to the mPFC (Fig. 5). We previously reported a group of cholinergic neurons that simultaneously projects to the mPFC and limbic thalamus[46]. The collateral projection pattern could be a common pattern of the cholinergic neurons and non-cholinergic neurons in the basal forebrain, in which case neurons in the basal forebrain can precisely regulate neurons in the mPFC and the

upstream neurons in the thalamus to control the synchronous discharge of two brain areas.

Second, many upstream brain areas of the mPFC also project to the AM. Specifically, neurons in the AM targeting mPFC can receive direct inputs from the dorsal striatum (Fig. 5g). In the canonical basal ganglia circuits, the information from the cortex passes through the dorsal striatum and flows all the way to the reticular part of the substantia nigra via the direct and indirect pathways; the substantia nigra, reticular part subsequently sends projections to the thalamus and the information is ultimately transmitted back to the cortex through the thalamic nuclei[47]. Our findings suggest that information can also be transmitted through an mPFC–dorsal striatum–thalamus–mPFC hyper-direct pathway.

Single-neuron projections from cortical and hippocampal areas. The neocortex provides the most long-range inputs to SST+, PV+ and VIP+ neurons in the mPFC. The distribution of input neurons in the neocortex is area-dependent. In the agranular cortex, such as the limbic cortex, motor cortex and associative cortex, the input neurons predominantly reside in layers II and III, while in the granular cortex, such as the sensory cortex, the input neurons are mainly found in layer V. This finding suggests that there may be a fundamental difference in the mechanism of information flow between the agranular cortex to the mPFC and the granular cortex to the mPFC, and differences between layers II and III neurons in the agranular cortex and the granular cortex.

We reconstructed the morphology and projectome of 86 cortical neurons and 33 hippocampal neurons. Based on the projection logic, we identified several types of cortical and hippocampal input neurons. Most mPFC-projecting neurons have collaterals to different brain areas in non-random combinations, indicating that when the information flows from one brain area to the mPFC, other brain areas may receive the same information in parallel.

In cortical areas, we identified at least seven types of cortical neurons in layers II, III, V and VI that project to GABAergic neurons in the mPFC (Figs. 6 and 7). Each type of cortical neuron has unique dendritic and axonal arborizations. Our data provide insights into the diversity of cortical neurons. It is well known that other cortical areas connect with the prefrontal cortex through bottom-up and top-down modulation[48]. The diversity of the cortical neurons that project to different GABAergic neurons in the mPFC implies that each type of neuron may transfer different information to carry out different functions.

Similarly, we found that some hippocampal pyramidal neurons that target different GABAergic neurons in the mPFC also display unique collateral projection patterns (Fig. 8). The different projection patterns of the upstream hippocampal pyramidal neurons suggest that the hippocampus-PV+$_{mPFC}$ circuitry and the hippocampus-SST+$_{mPFC}$ circuitry may have different functions.

Limitations of the present study. This study has several potential limitations. First, we used the two helper virus system, which may result in overestimation of the number of true starter cells[49], as some dual-color-labeled neurons may only express TVA but not RG. Second, we used the original version of the TVA receptor. This may cause wider spreading of the starter cells and some non-specific expression of the TVA receptor at the injection site[18], making it difficult to analyze local circuits. However, analysis of the starter-cell center of mass (COM) suggested that starter cells in PL-targeting samples and ILA-targeting samples were mostly separated. In future studies, using the modified version of the TVA receptor (TC66T) may be more effective at restricting starter cells to individual regions and specific cell types[18]. However, our control experiments showed that the long-range input labeling was nevertheless cell-type specific, indicating that the conclusions drawn in the present study are robust. Third, our immunochemical results showed that 8–10% of starter cells are not restricted to specific cell types, which was similar to previous studies[50]. There are maybe two reasons for these unrestricted neurons: the low immunogenicity of a few starter cells[49] and a few Cre-positive neurons expressing the specific markers during development but not in adulthood.

A recent report also mapped the whole-brain afferent distributions of four neuron types in the mPFC[49]. The overall patterns and respective weights of input neurons in the main brain areas were similar across our studies. However, in some brain areas, the input biases we found were not present in the previous study. These differences were probably caused by the variability of RV labeling and the different distributions of the starter cells. Furthermore, in the previous study, a single helper virus was used for monosynaptic RV tracing, which made the analysis of local connectivity available. In the present study we took advantage of the precise whole-brain imaging system and provided a more comprehensive analysis of the long-range input neurons.

In general, our study provides an atlas of long-range inputs to PV+, SST+ and VIP+ neurons in the mPFC. This atlas contains information regarding not only the distribution but also the neurochemical properties and fine morphology of input neurons. This atlas can facilitate the modeling and understanding of the functional differences of different GABAergic neurons in the mPFC, which may, in turn, shed light on the treatment of mental disorders associated with mPFC dysfunction.

Online content

Any methods, additional references, Nature Research reporting summaries, source data, statements of code and data availability and associated accession codes are available at https://doi.org/10.1038/s41593-019-0429-9.

References

1. Pinto, L. & Dan, Y. Cell-type-specific activity in prefrontal cortex during goal-directed behavior. *Neuron* **87**, 437–450 (2015).
2. Kvitsiani, D. et al. Distinct behavioural and network correlates of two interneuron types in prefrontal cortex. *Nature* **498**, 363–366 (2013).
3. Croarkin, P. E., Levinson, A. J. & Daskalakis, Z. J. Evidence for GABAergic inhibitory deficits in major depressive disorder. *Neurosci. Biobehav. Rev.* **35**, 818–825 (2011).
4. Lewis, D. A., Hashimoto, T. & Volk, D. W. Cortical inhibitory neurons and schizophrenia. *Nat. Rev. Neurosci.* **6**, 312–324 (2005).
5. Khoshkhoo, S., Vogt, D. & Sohal, V. S. Dynamic, cell-type-specific roles for GABAergic interneurons in a mouse model of optogenetically inducible seizures. *Neuron* **93**, 291–298 (2017).
6. Tremblay, R., Lee, S. & Rudy, B. GABAergic interneurons in the Neocortex: from cellular properties to circuits. *Neuron* **91**, 260–292 (2016).
7. Hoover, W. B. & Vertes, R. P. Anatomical analysis of afferent projections to the medial prefrontal cortex in the rat. *Brain Struct. Funct.* **212**, 149–179 (2007).
8. Zingg, B. et al. Neural networks of the mouse neocortex. *Cell* **156**, 1096–1111 (2014).
9. Oh, S. W. et al. A mesoscale connectome of the mouse brain. *Nature* **508**, 207–214 (2014).
10. Kim, T. et al. Cortically projecting basal forebrain parvalbumin neurons regulate cortical gamma band oscillations. *Proc. Natl Acad. Sci. USA* **112**, 3535–3540 (2015).
11. Kabanova, A. et al. Function and developmental origin of a mesocortical inhibitory circuit. *Nat. Neurosci.* **18**, 872–882 (2015).
12. Delevich, K., Tucciarone, J., Huang, Z. J. & Li, B. The mediodorsal thalamus drives feedforward inhibition in the anterior cingulate cortex via parvalbumin interneurons. *J. Neurosci.* **35**, 5743–5753 (2015).
13. Wickersham, I. R. et al. Monosynaptic restriction of transsynaptic tracing from single, genetically targeted neurons. *Neuron* **53**, 639–647 (2007).
14. Wall, N. R., Wickersham, I. R., Cetin, A., De La Parra, M. & Callaway, E. M. Monosynaptic circuit tracing in vivo through Cre-dependent targeting and complementation of modified rabies virus. *Proc. Natl Acad. Sci. USA* **107**, 21848–21853 (2010).
15. Gong, H. et al. High-throughput dual-colour precision imaging for brain-wide connectome with cytoarchitectonic landmarks at the cellular level. *Nat. Commun.* **7**, 12142 (2016).

16. Kim, J., Pignatelli, M., Xu, S. Y., Itohara, S. & Tonegawa, S. Antagonistic negative and positive neurons of the basolateral amygdala. *Nat. Neurosci.* **19**, 1636–1646 (2016).

17. Watabe-Uchida, M., Zhu, L. S., Ogawa, S. K., Vamanrao, A. & Uchida, N. Whole-brain mapping of direct inputs to midbrain dopamine neurons. *Neuron* **74**, 858–873 (2012).

18. Miyamichi, K. et al. Dissecting local circuits: parvalbumin interneurons underlie broad feedback control of olfactory bulb output. *Neuron* **80**, 1232–1245 (2013).

19. Ohara, S. et al. Dual transneuronal tracing in the rat entorhinal-hippocampal circuit by intracerebral injection of recombinant rabies virus vectors. *Front. Neuroanat.* **3**, 1 (2009).

20. DeNardo, L. A., Berns, D. S., DeLoach, K. & Luo, L. Q. Connectivity of mouse somatosensory and prefrontal cortex examined with trans-synaptic tracing. *Nat. Neurosci.* **18**, 1687–1697 (2015).

21. Beier, K. T. et al. Circuit architecture of VTA dopamine neurons revealed by systematic input-output mapping. *Cell* **162**, 622–634 (2015).

22. Beier, K. T. et al. Topological organization of ventral tegmental area connectivity revealed by viral-genetic dissection of input−output relations. *Cell Rep.* **26**, 159–167 (2019).

23. Picciotto, M. R., Higley, M. J. & Mineur, Y. S. Acetylcholine as a neuromodulator: cholinergic signaling shapes nervous system function and behavior. *Neuron* **76**, 116–129 (2012).

24. Lesch, K. P. & Waider, J. Serotonin in the modulation of neural plasticity and networks: implications for neurodevelopmental disorders. *Neuron* **76**, 175–191 (2012).

25. Zaborszky, L. et al. Neurons in the basal forebrain project to the cortex in a complex topographic organization that reflects corticocortical connectivity patterns: an experimental study based on retrograde tracing and 3D reconstruction. *Cereb. Cortex* **25**, 118–137 (2015).

26. Conti, F., DeBiasi, S., Minelli, A., Rothstein, J. D. & Melone, M. EAAC1, a high-affinity glutamate transporter, is localized to astrocytes and gabaergic neurons besides pyramidal cells in the rat cerebral cortex. *Cereb. Cortex* **8**, 108–116 (1998).

27. Ren, J. et al. Anatomically defined and functionally distinct dorsal raphe serotonin sub-systems. *Cell* **175**, 472–487 (2018).

28. Saunders, A., Granger, A. J. & Sabatini, B. L. Corelease of acetylcholine and GABA from cholinergic forebrain neurons. *eLife* **4**, e06412 (2015).

29. Liu, Z. X. et al. Dorsal raphe neurons signal reward through 5-HT and glutamate. *Neuron* **81**, 1360–1374 (2014).

30. Tamamaki, N. et al. Green fluorescent protein expression and colocalization with calretinin, parvalbumin, and somatostatin in the GAD67-GFP knock-in mouse. *J. Comp. Neurol.* **467**, 60–79 (2003).

31. Schwarz, L. A. et al. Viral-genetic tracing of the input-output organization of a central noradrenaline circuit. *Nature* **524**, 88–92 (2015).

32. Larsen, D. D., Wickersham, I. R. & Callaway, E. M. Retrograde tracing with recombinant rabies virus reveals correlations between projection targets and dendritic architecture in layer 5 of mouse barrel cortex. *Front. Neural Circuits* **1**, 5 (2008).

33. Rock, C., Zurita, H., Lebby, S., Wilson, C. J. & Apicella, A. J. Cortical circuits of callosal GABAergic neurons. *Cereb. Cortex* **28**, 1154–1167 (2018).

34. Economo, M. N. et al. Distinct descending motor cortex pathways and their roles in movement. *Nature* **563**, 79–84 (2018).

35. van Aerde, K. I. & Feldmeyer, D. Morphological and physiological characterization of pyramidal neuron subtypes in rat medial prefrontal cortex. *Cereb. Cortex* **25**, 788–805 (2015).

36. Spellman, T. et al. Hippocampal-prefrontal input supports spatial encoding in working memory. *Nature* **522**, 309–314 (2015).

37. Padilla-Coreano, N. et al. Direct ventral hippocampal-prefrontal input is required for anxiety-related neural activity and behavior. *Neuron* **89**, 857–866 (2016).

38. Soltesz, I. & Losonczy, A. CA1 pyramidal cell diversity enabling parallel information processing in the hippocampus. *Nat. Neurosci.* **21**, 484–493 (2018).

39. Fanselow, M. S. & Dong, H. W. Are the dorsal and ventral hippocampus functionally distinct structures? *Neuron* **65**, 7–19 (2010).

40. Abbas, A. I. et al. Somatostatin interneurons facilitate hippocampal-prefrontal synchrony and prefrontal spatial encoding. *Neuron* **100**, 926–939 (2018).

41. Hoover, W. B. & Vertes, R. P. Projections of the medial orbital and ventral orbital cortex in the rat. *J. Comp. Neurol.* **519**, 3766–3801 (2011).

42. Ballinger, E. C., Ananth, M., Talmage, D. A. & Role, L. W. Basal forebrain cholinergic circuits and signaling in cognition and cognitive decline. *Neuron* **91**, 1199–1218 (2016).

43. Szonyi, A. et al. The ascending median raphe projections are mainly glutamatergic in the mouse forebrain. *Brain Struct. Funct.* **221**, 735–751 (2016).

44. Allen, T. G. J., Abogadie, F. C. & Brown, D. A. Simultaneous release of glutamate and acetylcholine from single magnocellular 'cholinergic' basal forebrain neurons. *J. Neurosci.* **26**, 1588–1595 (2006).

45. Kim, J. H. et al. Selectivity of neuromodulatory projections from the basal forebrain and locus ceruleus to primary sensory cortices. *J. Neurosci.* **36**, 5314–5327 (2016).

46. Li, X. N. et al. Generation of a whole-brain atlas for the cholinergic system and mesoscopic projectome analysis of basal forebrain cholinergic neurons. *Proc. Natl Acad. Sci. USA* **115**, 415–420 (2018).

47. Wei, W. & Wang, X. J. Inhibitory control in the cortico-basal ganglia-thalamocortical loop: complex regulation and interplay with memory and decision processes. *Neuron* **92**, 1093–1105 (2016).

48. Zhang, S. Y. et al. Organization of long-range inputs and outputs of frontal cortex for top-down control. *Nat. Neurosci.* **19**, 1733–1742 (2016).

49. Ahrlund-Richter, S. et al. A whole-brain atlas of monosynaptic input targeting four different cell types in the medial prefrontal cortex of the mouse. *Nat. Neurosci.* **22**, 657–668 (2019).

50. Taniguchi, H. et al. A resource of cre driver lines for genetic targeting of GABAergic neurons in cerebral cortex. *Neuron* **71**, 995–1013 (2011).

Author contributions

Q.L. and H.G. conceived and designed the study. Q.S., X.L. and M.R. performed the tracing experiments. Y.R. and M.L. performed the physiological experiments. Q.Z., X.Z., C.Z. and J.Y. performed the whole-brain data acquisition. M.Z., H.N. and A.L. performed the imaging processing. Q.S., M.R., P.L. and X.L. performed the neuron reconstruction. Q.S., X.L., H.G. and Q.L. wrote the paper.

Competing interests

The authors declare no competing interests.

Additional information

Supplementary information is available for this paper at https://doi.org/10.1038/s41593-019-0429-9.

Reprints and permissions information is available at www.nature.com/reprints.

Correspondence and requests for materials should be addressed to Q.L.

Peer review information: *Nature Neuroscience* thanks Ian Wickersham and the other, anonymous, reviewer(s) for their contribution to the peer review of this work.

Methods

Animals. In the RV-tracing experiments, C57BL/6J, PV-Cre[51], SST-Cre, VIP-Cre[50] and Ai14 reporter line[51] adult male mice (2–6 months) were used. In the electrophysiology experiments, chat-Cre[51] and sert-Cre[52] mice were crossed with GAD67-GFP mice[30]. Three-month hybrid F1 male mice were used in the experiments. Mice were housed under conditions of 22 ± 1 °C and $55 \pm 5\%$ humidity with food and water ad libitum. Animal experiments were conducted in accordance with the Institutional Animal Ethics Committee of Huazhong University of Science and Technology.

Virus. The AAV8-CAG-FLEx-glycoprotein[17] (3.3×10^{12} genome copies (gc) ml⁻¹) and AAV8-EF1a -FLEx-TVA-mCherry[17] (8×10^{12} gc ml⁻¹) were purchased from the UNC Vector Core. The CAV2-Cre[31] (3×10^{12} gc ml⁻¹) were purchased from Montpellier vectorology. The AAV2/9-EF1a-DIO-histone-BFP-2A-TVA (4.2×10^{12} gc ml⁻¹), AAV2/9-EF1a-DIO-GFP-TVA[53] (3×10^{12} gc ml⁻¹), AAV2/9-EF1a-DIO-hCHR2(H134R)-YFP (2×10^{12} gc ml⁻¹), SAD-ΔG-GFP(EnvA)-RV (5×10^{8} international units (IU) ml⁻¹) and SAD-ΔG-DsRed(EnvA)-RV[53] (5×10^{8} IU ml⁻¹) were purchased from BrainVTA.

Stereotactic injections. For retrograde monosynaptic tracing, 150 nl of viral cocktail (1:2) containing AAV8-EF1a-FLEx-TVA-mCherry (this formula is also used with other AAV helper viruses expressing GFP or blue fluorescent protein (BFP)) and AAV8-CAG-FLEx-glycoprotein was injected into either the PL (bregma 1.9 mm, lateral 0.3 mm, depth 2.3 mm from skull surface) or the ILA area (bregma 1.4 mm, lateral 0.3 mm, depth 2.8 mm from skull surface) of PV-Cre, SST-Cre and VIP-Cre mice. Three weeks later, 300–400 nl of SAD-ΔG-GFP(EnvA)-RV or SAD-ΔG-DsRed(EnvA)-RV was injected into the same site. For cTRIO tracing related to Fig. 5h–j, 150 nl of viral cocktail (1:2) containing AAV2/9-EF1a-DIO-GFP-TVA and AAV8-CAG-FLEx-glycoprotein was injected into the AM (bregma 0.6 mm, lateral 0.5 mm, depth 3.75 mm from skull surface) of C57 mice, and 300 nl of CAV2-Cre was injected into the prelimbic area (bregma 1.9 mm, lateral 0.3 mm, depth 2.3 mm from skull surface) at the same time. Three weeks later, SAD-ΔG-dsRed(EnvA)-RV was injected into the prelimbic area. For cTRIO tracing related to Fig. 5l–n, 150 nl of viral cocktail (1:2) containing AAV8-EF1a-FLEx-TVA-mCherry and AAV8-CAG-FLEx-glycoprotein was injected into the AM (bregma 0.6 mm, lateral 0.5 mm, depth 3.75 mm from skull surface) of Ai14 mice, and 300 nl of CAV2-Cre was injected into the prelimbic area (bregma 1.9 mm, lateral 0.3 mm, depth 2.3 mm from skull surface) at the same time. Three weeks later, SAD-ΔG-GFP(EnvA)-RV was injected into the AM. For electrophysiology experiments, 300 nl of AAV2/9-EF1a-DIO-hCHR2(H134R)-YFP was injected into the diagonal band nucleus (VDB, bregma 0.86 mm, lateral 0 mm, depth 4.75 mm from skull surface; HDB, bregma 0.3 mm, lateral 1.2 mm, depth 5.3 mm from skull surface) of chat-Cre:GAD67-GFP mice or the raphe nuclei (dorsal nucleus raphe (DR), bregma 4.8 mm, lateral 0 mm, depth 3 mm from skull surface; superior central nucleus raphe (CS), bregma 4.8 mm, lateral 0 mm, depth 4.5 mm from skull surface) of sert-Cre:GAD67-GFP mice. After 3–4 weeks, the electrophysiology experiments were performed. For CTB retrograde studies, 200–300 nl of conjugated CTb (Life Technologies) was injected unilaterally in the PL area (bregma 1.9 mm, lateral 0.3 mm, depth 2.3 mm from skull surface) or the ILA area (bregma 1.4 mm, lateral 0.3 mm, depth 2.8 mm from skull surface) of C57 mice. All the viruses were delivered by a sharp micropipette mounted on a Nanoject II (Drummond Scientific) attached to a micromanipulator and then injected at a speed of 60 nl min⁻¹. The glass micropipette was held for an extra 10 min after the completion of the injection and then slowly retreated. After the surgery, the incisions were stitched and lincomycin hydrochloride and lidocaine hydrochloride gel was applied to prevent inflammation and alleviate pain for the animals. The mice injected with RV or CTb were killed for analysis 1 week after the injection.

Histology. Mice were deeply anesthetized with sodium pentobarbital (1% wt/vol) and subsequently intracardially perfused with 0.01 M PBS (Sigma-Aldrich), followed by 4% paraformaldehyde (Sigma-Aldrich) and 2.5% sucrose in 0.01 M PBS. The brains were excised and post-fixed in 4% paraformaldehyde at 4 °C for 12 h. For whole-brain imaging[15], the intact brain was embedded in glycol methacrylate (GMA) resin. The embedding protocol has been previously described[51]; briefly, each intact brain was rinsed overnight at 4 °C in a 0.01 M PBS solution and subsequently dehydrated in a graded ethanol series (50, 70 and 95% ethanol, changing from one concentration to the next every 1 h at 4 °C). After dehydration, the brains were immersed in a graded GMA series (Ted Pella Inc.), including 0.2% SBB (Sudan black B) (70, 85 and 100% GMA for 2 h each and 100% GMA overnight at 4 °C). Subsequently, the samples were impregnated in a prepolymerization GMA solution for 3 d at 4 °C and embedded in a vacuum oven at 48 °C for 24 h. Each 100 g of GMA solution (100%) consisted of two resin components (A component, 67 g; B component, 29.4 g), 2.8 g of deionized water, 0.2 g of SBB, and 0.6 g of AIBN (2,2′-azo-bis-butyronitrile) as an initiator. The 70 and 85% GMA solutions (wt/wt) were prepared from 95% ethanol and 100% GMA.

For double immunohistochemistry, the fixed brains were embedded by oxidized agarose and the embedding protocol has been described elsewhere[54]. Briefly, agarose type I (Sigma) was oxidized by stirring in 10 mM sodium periodate (NaIO₄, Sigma) solution for 2 h at room temperature (20–25 °C); then

the oxidized agarose was washed three times in 0.01 M PBS (Sigma-Aldrich Inc.) and resuspended in 0.01 M PBS to bring the final concentration to 5%. The mouse brain was pat-dried and embedded in melted oxidized agarose using a cube-shaped mold and put in a 4 °C refrigerator for solidification. Then the mouse brain was sectioned at 50 μm on a vibration microtome (Leica, VT1200S). The sections of interest were blocked with 5% (wt/vol) BSA containing 0.3% Triton-X 100 (vol/vol) in 0.01 M PBS for 1 h, and then incubated with the following primary antibodies (12 h at 4 °C): anti-PV (1:1,000, mouse, Millipore, MAB1572), anti-SST (1:200, goat, Santa Cruz, sc-7819), anti-chat (1:500, goat, Millipore, AB144P), anti-chat (1:500, rabbit, Millipore, AB143), anti-PV (1:1,000, mouse, Millipore, MAB1572), anti-chat (1:500, rabbit, Millipore, AB143), anti-EAAC1 (1:500, goat, Millipore, AB1520), anti-TH (1:1,000, rabbit, Sigma-Aldrich, T8700-1VL), anti-EAAC1 (1:500, goat, Millipore, AB1520), anti-TPH2 (1:1,000, rabbit, Thermo, PA1-778) and anti-EAAC1 (1:500, goat, Millipore, AB1520). After rinsing, sections were incubated with the following fluorophore-conjugated secondary antibody for 2 h at room temperature (1:500; Invitrogen): Alexa Fluor 405, Gt-Anti-Mouse, H; Alexa Fluor 647, Rb-Anti-Gt, H+L; Alexa Fluor 594, Gt-Anti-Rabbit, H and Alexa Fluor 405, Gt-Anti-Mouse, H; Alexa Fluor 568, Donkey-Anti-Rabbit, H and Alexa Fluor 647, Donkey-Anti-Goat, H. Antibodies were diluted in the same block solution. See also Supplementary Table 14 for detailed antibody information.

Slice physiology. The methods of slice preparation, whole-cell patch recording and photostimulation were similar to those described elsewhere[29,55]. AAV-DIO-ChR2-YFP virus was injected into the raphe nuclei of Gad67-GFP::Sert-Cre mice and the basal forebrain of Gad67-GFP::Chat-Cre. After 3 weeks of recovery, the mice were deeply anesthetized with pentobarbital (100 mg kg⁻¹ intraperitoneal) and then transcardially perfused with ice-cold oxygenated perfusion solution (5 ml, 0.5 ml s⁻¹). The perfusion solution contained the following (in mM): 225 sucrose, 119 NaCl, 2.5 KCl, 1 NaH₂PO₄, 4.9 MgCl₂, 0.1 CaCl₂, 26.2 NaHCO₃, 1.25 glucose, 3 kynurenic acid, and 1 sodium ascorbate. After perfusion, the mouse brain was dissected out and placed into ice-cold oxygenated slicing solution. The slicing solution contained the following (in mM): 110 choline chloride, 2.5 KCl, 0.5 CaCl₂, 7 MgCl₂, 1.3 NaH₂PO₄, 25 NaHCO₃, 10 glucose, 1.3 sodium ascorbate and 0.6 sodium pyruvate. Coronal sections (200 μm) were cut with vibratome (VT1200s, Leica). The slices were incubated for 1 h at 34 °C in oxygenated artificial cerebrospinal fluid (aCSF) saturated with 95% O₂/5% CO₂ that contained the following (in mM): 125 NaCl, 2.5 KCl, 2 CaCl₂, 1.3 MgCl₂, 1.3 NaH₂PO₄, 1.3 sodium ascorbate, 0.6 sodium pyruvate, 10 glucose and 25 NaHCO₃. The brain slices were transferred to a recording chamber at room temperature for recordings. All chemicals used in the slice preparation were purchased from Sigma (St Louis).

Neurons in the mPFC were recognized based on the expression of GFP fluorescence in somata. The internal solution within whole-cell recording pipettes (3–5 MΩ) contained (in mM): 130 potassium gluconate, 10 HEPES, 0.6 EGTA, 5 KCl, 3 Na₂ATP, 0.3 Na₃GTP, 4 MgCl₂ and 10 Na₂ phosphocreatine (pH 7.2–7.4). Voltage-clamp and current-clamp recordings were performed using a MultiClamp700B amplifier (Molecular Devices). For voltage-clamp recordings, the neurons were held at −65 mV. Traces were low-pass filtered at 2.6 kHz and digitized at 10 kHz (DigiData 1440, Molecular Devices). The data were acquired and analyzed using Clampfit v.10.0 software (Molecular Devices). For light stimulation, the tip of an optical fiber (200 μm core diameter, 0.22 numerical aperture (NA)) coupled to a 473-nm laser was submerged in aCSF and placed ~300 μm from the recording site. The delivery of light pulses (5 ms, 0.2–20 mW mm⁻²) was controlled through digital commands from the Digidata 1440 digitizer. For drug application, DNQX (10 μM, Sigma), hexamethonium-Cl (HMT, 50 μM; Sigma) and mecamylamine (Mec, 5 μM; Sigma) were added to the superfusion medium through the dilution of stock solutions.

Microscopy. For starter-cell counting, the sections containing starter cells were mounted with 50% glycerol (vol/vol) and imaged at multiple focal planes using a ×10, 0.45 NA objective (Zeiss 710). For immunohistochemistry imaging, the sections were mounted with 50% glycerol (vol/vol) and imaged using a ×20, 0.75 NA objective (Zeiss 710). For whole-brain soma counting, all 50-μm sections obtained from mouse brains were collected and mounted with 50% glycerol containing propidium iodide (PI, 1 μg ml⁻¹, wt/vol), then scanned using a ×4, 0.2 NA objective (Nikon Ni-E). For the dual-color RV imaging shown in Fig. 8, the sections were mounted with 50% glycerol (vol/vol) and imaged using a ×10, 0.45 NA objective (Olympus versus 120 virtual microscopy slide scanning system, Olympus). For dual-color CTb imaging, all 50-μm sections obtained from mouse brains were collected and mounted with 50% glycerol. Every third section was imaged using a ×10, 0.45 NA objective (Zeiss 710). For whole-brain precise imaging, the GMA embedded mouse brains were imaged by our home-made fMOST system. The imaging system has been described previously[28]. Briefly, the system used a mercury lamp (X-Cite exacte, Lumen Dynamics) as light source, a digital micro-mirror device (DMD, XD-ED01N, X-digit) to generate the illumination grid pattern and a water immersion objective (1.0 NA, XLUMPLFLN 20XW, Olympus) for imaging. Two scientific complementary metal-oxide semiconductor cameras (ORCA-Flash 4.0, Hamamatsu Photonics K.K.) were used for signal detection. A piezoelectric translational stage (P-725 PIFOC Long-Travel Objective Scanner, E-753 Digital Piezo Controller, PI GmbH) moved the

objective for axial scanning. The sample box was screwed onto a high-precision 3D translation stage (ABL20020-ANT130-AVL125, Aerotech Inc.). The 3D translation stage moved the sample for mosaic scanning and sectioning. A diamond knife (Diatome AG) was used for sample sectioning. During imaging, the sample was immersed in a water bath containing PI ($1\,\mu g\,ml^{-1}$, wt/vol) and $0.05\,M\,Na_2CO_3$. The objective scanned the surface of the sample in mosaic mode at a step of $2\,\mu m$. After one surface was finished, the diamond knife removed the imaged surface and exposed the smooth fresh surface for imaging. The mosaic imaging process was repeated until the entire coronal section was acquired.

Image preprocessing. The raw data acquired by the brain positioning system needed image preprocessing for mosaic stitching and illumination correction. This process has been described before[15]. Briefly, the mosaics of each coronal section were stitched to obtain an entire section based on accurate spatial orientation and adjacent overlap. Lateral illumination correction was performed section by section. Image preprocessing was implemented in C++ and optimized in parallel using the Intel MPI Library (v.3.2.2.006, Intel). The whole data sets were executed on a computing server (72 cores, 2 GHz per core) within 6 h.

Visualization and reconstruction. We visualized the data set using Amira software (v.5.2.2, FEI) to generate the figures and videos. The data set acquired by the dual-color precise imaging system was separated into the GFP channel and PI channel. The PI-labeled data set was sampled to $3.2 \times 3.2 \times 50\,\mu m^3$ and imported into Amira to generate the outline of the mouse brain. To trace the morphology of the input neurons, we transformed the data format of GFP-labeled data from TIFF to LDA type via Amira and applied the filament editor module to trace the morphology of GFP-labeled neurons at the whole-brain level by human–machine interaction. Briefly, we loaded the data block of interests into Amira and assigned the initial and terminal points of the fibers in the block, so that Amira could automatically calculate the pathway between initial and terminal points. We repeated this procedure until the reconstruction was finished. The reconstructed neurons were checked back-to-back by three persons. The tracing results was saved in SWC format. We loaded the outline of the mouse brain and the tracing results into Amira simultaneously and used the moviemaker module of Amira to generate figures and videos.

Cell counting and registration. For starter-cell counting, the starter cells were manually counted using the Cell Counter ImageJ plug-in. For whole-brain input neuron counting, the input neurons were either manually counted using the Cell Counter ImageJ plug-in with reference to the Allen brain atlas or automatically identified by NeuroGPS[56]. The distribution of the input neurons in 41 discrete brain regions across the entire extent of the whole brain were quantified. The methods of the registration have been described elsewhere[57]. Briefly, to align our map with the existing atlas, the data set was rotated and resampled to a voxel resolution of $10 \times 10 \times 10\,\mu m^3$ for registering in the template data set of Allen CCF v3.0 (ref. [58]; Supplementary Table 15). Then, we manually segmented several brain regions as landmarks. Finally, we registered our results in the Allen CCF v.3.0 and loaded the outline of the mouse brain and the results into Amira simultaneously to generate figures.

Starter-cell COM and regression analysis. The determination of starter-cell COM was similar to that in a previous study[22]. The mean vertical distance of the starter cells to the midline, brain surface and the coronal plane under the bregma point were manually measured in ImageJ and according to the Allen brain CCF. Linear regression analysis with mean vertical distance to the midline, brain surface and the coronal plane under the bregma point was processed by Graphpad Prism v.6.01. Linear regression analysis with COM and Cre lines was performed in MATLAB, where input site percentages were dependent variables, COMs were

predictors and driver strains were categorical predictors. The fitted models were then analyzed using ANOVA to report the R^2 values to indicate how well the percentage for each input site could be explained by each combination of predictor variables.

Statistics. All statistical graphs were generated using Graphpad Prism v.6.01. The two-tailed Student's *t*-test and one-way ANOVA followed by Tukey's post hoc tests were also performed using Graphpad Prism v.6.01 and SPSS (IBM SPSS Statistics 23). The confidence level was set to 0.05 (*P* value) and all results were presented as the means ± s.e.m. All the individual data points were shown in the histograms and no data points were excluded from the analyses. The data distribution was assumed to be normal but this was not formally tested.

Sample sizes statement. No statistical methods were used to predetermine sample size; however, the sample size was similar to previous studies[20,48].

Replication. Results described throughout the paper were reproduced. Multiple rounds of experimentation were required, that is, from multiple mice. No results were included that were not observed in multiple animals. No issues were identified in replicating any of the reported findings.

Randomization. Animals were not randomized due to the necessity of a genetic construct (PV-Cre, SST-Cre, VIP-Cre mice).

Blinding. Investigators were not blind to subject groups because knowledge of experimental conditions was required during data collection and evaluation.

Reporting Summary. Further information on research design is available in the Nature Research Reporting Summary linked to this article.

Data availability

The data that support the findings of this study are available in the Supplementary Tables and from the corresponding author upon reasonable request. Data including the whole-brain distribution of the input neurons and the reconstructions of the neural morphology in the neocortex and hippocampus can be accessed at http://atlas.brainsmatics.org/a/sun1903.

References

51. Madisen, L. et al. A robust and high-throughput Cre reporting and characterization system for the whole mouse brain. *Nat. Neurosci.* **13**, 133–140 (2010).
52. Zhuang, X., Masson, J., Gingrich, J. A., Rayport, S. & Hen, R. Targeted gene expression in dopamine and serotonin neurons of the mouse brain. *J. Neurosci. Methods* **143**, 27–32 (2005).
53. Zhang, Z. et al. Whole-brain mapping of the inputs and outputs of the medial part of the olfactory tubercle. *Front Neural Circuits* **11**, 52 (2017).
54. Ragan, T. et al. Serial two-photon tomography for automated ex vivo mouse brain imaging. *Nat. Methods* **9**, 255–258 (2012).
55. Zhang, J. et al. Presynaptic excitation via GABAB receptors in habenula cholinergic neurons regulates fear memory expression. *Cell* **166**, 716–728 (2016).
56. Peng, J. et al. A quantitative analysis of the distribution of CRH neurons in whole mouse brain. *Front Neuroanat.* **11**, 63 (2017).
57. Ni H., et al. A robust image registration interface for large volume brain atlas. Preprint at *bioRxiv* https://doi.org/10.1101/377044 (2018).
58. Kuan, L. et al. Neuroinformatics of the allen mouse brain connectivity atlas. *Methods* **73**, 4–17 (2015).

naturereserach

Corresponding author(s):   Qingming Luo

Last updated by author(s):   May 6, 2019

Reporting Summary

Nature Research wishes to improve the reproducibility of the work that we publish. This form provides structure for consistency and transparency in reporting. For further information on Nature Research policies, see Authors & Referees and the Editorial Policy Checklist.

Statistics

For all statistical analyses, confirm that the following items are present in the figure legend, table legend, main text, or Methods section.

n/a	Confirmed	
☐	☒	The exact sample size (n) for each experimental group/condition, given as a discrete number and unit of measurement
☐	☒	A statement on whether measurements were taken from distinct samples or whether the same sample was measured repeatedly
☐	☒	The statistical test(s) used AND whether they are one- or two-sided *Only common tests should be described solely by name; describe more complex techniques in the Methods section.*
☒	☐	A description of all covariates tested
☐	☒	A description of any assumptions or corrections, such as tests of normality and adjustment for multiple comparisons
☐	☒	A full description of the statistical parameters including central tendency (e.g. means) or other basic estimates (e.g. regression coefficient) AND variation (e.g. standard deviation) or associated estimates of uncertainty (e.g. confidence intervals)
☐	☒	For null hypothesis testing, the test statistic (e.g. F, t, r) with confidence intervals, effect sizes, degrees of freedom and P value noted *Give P values as exact values whenever suitable.*
☒	☐	For Bayesian analysis, information on the choice of priors and Markov chain Monte Carlo settings
☒	☐	For hierarchical and complex designs, identification of the appropriate level for tests and full reporting of outcomes
☐	☒	Estimates of effect sizes (e.g. Cohen's d, Pearson's r), indicating how they were calculated

Our web collection on statistics for biologists contains articles on many of the points above.

Software and code

Policy information about availability of computer code

Data collection	The softwares and codes used for imaging, image preprocessing, visualization, reconstruction and registration in this study were similar to previous studies(Gong et al. 2016. Nat. Communications) and described in Supplementary Materials and Methods. The softwares and codes used for slice physiology were described elsewhere(Liu et al. 2014. Neuron; Zhang et al. 2016. Cell). Cell counting was performed by ImageJ 2.0 or NeuroGPS(Quan et al. 2013. Scientific Reports). Amira software (v 5.2.2, FEI, Me´rignac Cedex, France) was used for data visualization and neuron reconstruction.
Data analysis	MatLab (2018a) was used for regression analysis. Statistical analysis was performed using preset algorithms in Graphpad Prism (v.6) and SPSS (IBM SPSS Statistics 23).. Figures were prepared in Adobe Illustrator CS7. The online sunburst diagrams were created using the open online resource available at the Allen Institute for Brain Science (Lein, E.S., et al. Genome-wide atlas of gene expression in the adult mouse brain. Nature 445, 168-176 (2007)), and part of the computer code adapted from Zhang, S., et al. Organization of long-range inputs and outputs of frontal cortex for top-down control. Nature neuroscience 19, 1733-1742 (2016)

For manuscripts utilizing custom algorithms or software that are central to the research but not yet described in published literature, software must be made available to editors/reviewers. We strongly encourage code deposition in a community repository (e.g. GitHub). See the Nature Research guidelines for submitting code & software for further information.

Data

Policy information about availability of data

All manuscripts must include a data availability statement. This statement should provide the following information, where applicable:
- Accession codes, unique identifiers, or web links for publicly available datasets
- A list of figures that have associated raw data
- A description of any restrictions on data availability

The data that support the findings of this study are available in Supplementary tables and from the corresponding author upon reasonable request. The data can also be accessed on http://atlas.brainsmatics.org/a/sun1903.

Field-specific reporting

Please select the one below that is the best fit for your research. If you are not sure, read the appropriate sections before making your selection.

☒ Life sciences   ☐ Behavioural & social sciences   ☐ Ecological, evolutionary & environmental sciences

For a reference copy of the document with all sections, see nature.com/documents/nr-reporting-summary-flat.pdf

Life sciences study design

All studies must disclose on these points even when the disclosure is negative.

Sample size	No statistical methods were used to predetermine sample size, however the sample size was similar to previous studies(Laura A DeNardo et al. 2015. Nat. Neuroscience; Siyu Zhang et al. 2016. Nat. Neuroscience.)
Data exclusions	No animals were excluded from analysis.
Replication	Results described throughout the paper were reproduced. Multiple rounds of experimentation were required, i.e., from multiple mice. No results are included that were not observed in multiple animals. No issues were identified in replicating any of the reported findings.
Randomization	Animals were not randomized due to the necessity of a genetic construct (PV-Cre, SST-Cre, VIP-Cre mice).
Blinding	Investigators were not blind to subject groups because knowledge of experimental conditions was required during data collection and evaluation.

Reporting for specific materials, systems and methods

We require information from authors about some types of materials, experimental systems and methods used in many studies. Here, indicate whether each material, system or method listed is relevant to your study. If you are not sure if a list item applies to your research, read the appropriate section before selecting a response.

Materials & experimental systems

n/a	Involved in the study
☐	☒ Antibodies
☒	☐ Eukaryotic cell lines
☒	☐ Palaeontology
☐	☒ Animals and other organisms
☒	☐ Human research participants
☒	☐ Clinical data

Methods

n/a	Involved in the study
☒	☐ ChIP-seq
☒	☐ Flow cytometry
☒	☐ MRI-based neuroimaging

Antibodies

Antibodies used	All antibodies used in this work were described in Supplementary Materials and listed in Supplementary Table 14. Primary antibodies Host Target Company Catalogue # Dilution Manufacture Validation mouse Parvalbumin Millipore MAB1572 1:1000 "http://www.merckmillipore.com/CN/zh/product/Anti-Parvalbumin-Antibody,MM_NF-MAB1572" Goat "CholineAcetyltransferase" Millipore AB144P 1：500 "http://www.merckmillipore.com/CN/zh/product/Anti-Choline-Acetyltransferase-Antibody,MM_NF-AB144P" rabbit "CholineAcetyltransferase" Millipore AB143 1：500 "http://www.merckmillipore.com/CN/zh/product/Anti-Choline-Acetyltransferase-ChAT-Antibody,MM_NF-AB143" Goat "Neuronal Glutamate Transporter" Millipore AB1520 1：500 "http://www.merckmillipore.com/CN/zh/product/Anti-Glutamate-Transporter-Antibody-neuronal,MM_NF-AB1520" Goat Somatostatin Santa Cruz sc-7819 1:200 "https://www.scbt.com/scbt/product/somatostatin-antibody-d-20?requestFrom=search" rabbit Tyrosine Hydroxylase Sigma-Aldrich T8700-1VL 1：1000 "https://www.sigmaaldrich.com/catalog/product/sigma/t8700?lang=zh&region=CN" rabbit tryptophan hydroxylase 2 Thermo PA1-778 1：1000 "https://www.thermofisher.com/antibody/product/TPH2-Antibody-Polyclonal/PA1-778" Secondary antibodies Host Target Company Fluorophore Catalogue # Dilution Manufacture Validation Goat mouse Invitrogen Alexa Fluor 405 A-31553 1：500 "https://www.thermofisher.com/antibody/product/Goat-anti-Mouse-IgG-H-L-Cross-Adsorbed-Secondary-Antibody-Polyclonal/A-31553" rabbit Goat Invitrogen Alexa Fluor 647 A-21446 1：500 "https://www.thermofisher.com/antibody/product/Rabbit-anti-Goat-IgG-H-L-Cross-Adsorbed-Secondary-Antibody-Polyclonal/A-21446"

Goat rabbit Invitrogen Alexa Fluor 594 R37117 1：500 "https://www.thermofisher.com/antibody/product/Goat-anti-Rabbit-IgG-H-L-Cross-Adsorbed-Secondary-Antibody-Polyclonal/R37117"
Donkey rabbit Invitrogen Alexa Fluor 568 A10042 1：500 "https://www.thermofisher.com/antibody/product/Donkey-anti-Rabbit-IgG-H-L-Highly-Cross-Adsorbed-Secondary-Antibody-Polyclonal/A10042"
Donkey Goat Invitrogen Alexa Fluor 647 A-21447 1：500 "https://www.thermofisher.com/antibody/product/Donkey-anti-Goat-IgG-H-L-Cross-Adsorbed-Secondary-Antibody-Polyclonal/A-21447"

Validation	These are all well characterized commercial antibodies.The specificity of the primary and secondary antibodies was validated by the manufacturers. Validation profiles for all primary antibodies can be found in the links provided.

Animals and other organisms

Policy information about studies involving animals; ARRIVE guidelines recommended for reporting animal research

Laboratory animals	RV tracing experiments, C57BL/6J, PV-Cre, SST-Cre, VIP-Cre and Ai14 reporter line adult male mice(2-6 months) were used. Inelectrophysiology experiments, chat-Cre and sert-Cre mice were crossed with GAD67-GFP mice. The hybrid F1 male mice(2-3 months) were used in the experiments
Wild animals	No wild animals were used in this study.
Field-collected samples	No field samples were collected for analysis in this study.
Ethics oversight	Animal experiments were conducted in accordance with the Institutional Animal Ethics Committee of Huazhong University of Science and Technology.

Note that full information on the approval of the study protocol must also be provided in the manuscript.